JCI The Journal of Clinical Investigation

Targeting the αv integrin-TGF-β axis improves natural killer cell function against glioblastoma stem cells

Hila Shaim, … , Amy B. Heimberger, Katayoun Rezvani

J Clin Invest. 2021. https://doi.org/10.1172/JCI142116.

Research In-Press Preview **Immunology**

Graphical abstract

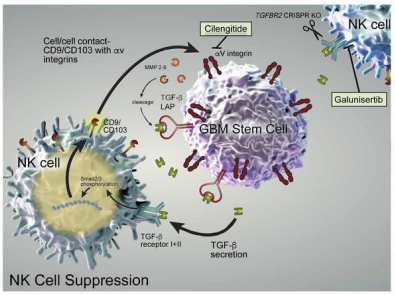

Targeting the αv integrin-TGF-β axis improves natural killer cell function against glioblastoma stem cells

Running title- GBM induce NK cell dysfunction via integrin-TGF-β axis

Authors

Hila Shaim[1,2+], Mayra Shanley[1+], Rafet Basar[1+], May Daher[1], Joy Gumin[3], Daniel Zamler[4], Nadima Uprety[1], Fang Wang[5], Yuefan Huang[5], Konrad Gabrusiewicz[3], Qi Miao[5], Jinzhuang Dou[5], Abdullah Alsuliman[1], Lucila N. Kerbauy[1], Sunil Acharya[1], Vakul Mohanty[5], Mayela Mendt[1], Sufang Li[1], Junjun Lu[1], Jun Wei[3], Natalie W. Fowlkes[6], Elif Gokdemir[1], Emily L. Ensley[1], Mecit Kaplan[1], Cynthia Kassab[3], Li Li[1], Gonca Ozcan[1], Pinaki P. Banerjee[1], Yifei Shen[5], April L. Gilbert[1], Corry M. Jones[1], Mustafa Bdiwi[1], Ana Karen Nunez Cortes[1], Enli Liu[1], Jun Yu[3], Nobuhiko Imahashi[1], Luis Muniz-Feliciano[1], Ye Li[1], Jian Hu[7], Giulio Draetta[4], David Marin[1], Dihua Yu[8], Stephan Mielke[2,9], Matthias Eyrich[10], Richard E. Champlin[1], Ken Chen[5], Frederick F. Lang[3], Elizabeth J. Shpall[1], Amy B. Heimberger[3+], Katayoun Rezvani[1+ *]

Affiliations

[1] Department of Stem Cell Transplantation and Cellular Therapy, The University of Texas MD Anderson Cancer Center, Houston, TX, USA

[2] Department of Internal Medicine II, University Medical Center Würzburg, Würzburg, Germany

[3] Department of Neurosurgery, The University of Texas MD Anderson Cancer Center, Houston, TX, USA

[4] Department of Genomic Medicine, The University of Texas MD Anderson Cancer Center, Houston, TX, USA

[5] Department of Bioinformatics and Computational Biology, The University of Texas MD Anderson Cancer Center, Houston, TX, USA

[6] Department of Veterinary Medicine and Surgery, The University of Texas MD Anderson Cancer Center, Houston, TX, USA

[7] Department of Cancer Biology, The University of Texas MD Anderson Cancer Center, Houston, TX, USA

[8] Department of Molecular and Cellular Oncology, The University of Texas MD Anderson Cancer Center, Houston, TX, USA

[9] Department of Hematology, Karolinska Institute, Stockholm, Sweden

[10] Department of Pediatric Hematology, Oncology and Stem Cell Transplantation, University Medical Center Würzburg, Würzburg, Germany

[+] These authors contributed equally to this paper.

* **Corresponding author**:

Katayoun Rezvani, email: krezvani@mdanderson.org

Department of Stem Cell Transplantation and Cellular Therapy, The University of Texas MD Anderson Cancer Center, Houston, TX, USA

ABSTRACT

Glioblastoma, the most aggressive brain cancer, recurs because glioblastoma stem cells (GSCs) are resistant to all standard therapies. We showed that GSCs, but not normal astrocytes, are sensitive to lysis by healthy allogeneic natural killer (NK) cells *in vitro*. Mass cytometry and single cell RNA sequencing of primary tumor samples revealed that glioblastoma-infiltrating NK cells acquired an altered phenotype associated with impaired lytic function relative to matched peripheral blood NK cells from glioblastoma patients or healthy donors. We attributed this immune evasion tactic to direct cell-cell contact between GSCs and NK cells via integrin-mediated TGF-β activation. Treatment of GSC-engrafted mice with allogeneic NK cells in combination with inhibitors of integrin or TGF-β signaling, or with *TGFBR2* gene-edited allogeneic NK cells prevented GSC-induced NK cell dysfunction and tumor growth. These findings revealed an important mechanism of NK cell immune evasion by GSCs and implicated the integrin-TGF-β axis as a potentially useful therapeutic target in glioblastoma.

INTRODUCTION

Glioblastoma multiforme (GBM) or grade IV astrocytoma, is the most common and aggressive type of primary brain tumor in adults. Despite current treatment with resection, radiotherapy and temozolamide*, the* outcome for this tumor is poor with a reported median survival of 14.6 months and a 2-year survival of 26.5% as the tumor invariably relapses (1). This dismal outcome has stimulated keen interest in immunotherapy as a means to circumvent one or more of the factors that have limited the impact of available treatments: (i) rapid growth rate of these aggressive tumors; (ii) their molecular heterogeneity and propensity to invade critical brain structures, and (iii) the tumor regenerative power of a small subset of glioblastoma stem cells (GSCs)(2, 3).

Emerging results from preclinical studies support the concept that not only mature GBM cells can be efficiently targeted by natural killer (NK) cells (4-8) but that their associated stem cells may also be highly susceptible to NK cell-mediated immune attack (9, 10). These innate lymphocytes have a broad role in protecting against tumor initiation and metastasis in many types of cancer, and they have distinct advantages over T cells as candidates for therapeutic manipulation (11, 12). However, the vast majority of tumor cells that have been studied to date possess formidable immune defenses, allowing them to evade NK cell-mediated cytotoxicity. These include disruption of receptor-ligand interactions between NK and tumor cells and the release of immunosuppressive cytokines into the microenvironment, such as transforming growth factor beta (TGF-β) (13-15). Even if one could shield NK cells from the evasive tactics of GBM tumors, it may not be possible to eradicate a sufficient number of self-renewing GSCs to sustain complete responses. Indeed, very little is known about the susceptibility of GSCs to NK cell surveillance *in vivo*. Thus, to determine if GSCs can be targeted by NK cells *in vivo*, we designed a preclinical study and used single cell analysis of primary GBM tissue from patients undergoing

surgery to determine the extent to which NK cells infiltrate sites of active tumor and the potency with which they eliminate patient-derived GSCs.

Using an experimental approach that allowed head-to-head comparison of NK cell markers at the single cell level in the peripheral blood and primary tumor specimens from patients with glioblastoma, we showed that NK cells have an altered phenotype that correlates with reduced NK cell cytolytic function. GSCs, which cause most recurrences of GBM tumor after therapy, proved highly susceptible to NK-mediated killing *in vitro*, but evaded NK cell recognition via a mechanism requiring direct αv integrin-mediated cell-cell contact, leading to the release and activation of TGF-β by the GCSs. In a patient-derived xenograft (PDX) orthotopic mouse model of glioblastoma, GSC-induced NK dysfunction was completely prevented by direct blockade of integrin or TGF-β or by CRISPR gene editing of the TGF-β receptor 2 (*TGFBR2*) on allogeneic NK cells, resulting in effective control of the tumor. Taken together, these data suggest that inhibition of the αv integrin-TGF-β axis could overcome a major obstacle to effective NK cell immunotherapy for GBM.

RESULTS

GSCs are susceptible to NK cell-mediated killing

GSCs can be distinguished from their mature tumor progeny at the transcriptional, epigenetic and metabolic levels (16, 17), raising the question of whether these cells can be recognized and killed by NK cells. We therefore asked whether patient-derived GSCs, defined as being capable of self-renewal, pluripotent differentiation, and tumorigenicity when implanted into an animal host, are susceptible to NK cell cytotoxic activity as compared with healthy human astrocytes. To answer this question, we performed a 4 hour ^{51}Chromium (^{51}Cr) release cytotoxicity assay. GSCs were derived from patients with various glioblastoma subtypes including mesenchymal (GSC17, GSC20, GSC267, GSC272), classical (GSC231, GSC6-27), and proneural (GSC8-11, GSC262) while also showing heterogeneity in the O (6)-Methylguanine-DNA methyltransferase (MGMT) methylation status (methylated: GSC231, GSC8-11, GSC267, GSC272; indeterminate: GSC6-27, GSC17, GSC262). The complete transcriptional profile for each GSC is summarized in **Supplemental Figure 1**. K562 targets were used as positive control because of their marked sensitivity to NK cell mediated killing due to lack of expression of HLA class I (18). Across all effector to target (E:T) ratios, healthy donor NK cells killed GSCs (n=6) and K562 cells with equal efficiency and much more readily than healthy human astrocytes (n=6), which displayed a relative resistance to NK cell-mediated killing **(Figure 1A)**. NK cells can also efficiently targeted non-GSC glioma cell lines such as U87 **(Figure 1A)**. Multi-parametric flow cytometry was then used to analyze the expression of NK cell activating or inhibitory receptor ligands on GSCs. GSCs (n=6) expressed normal levels of HLA-class I and HLA-E (both ligands for inhibitory NK receptors), at levels similar to those observed on healthy human astrocytes (n=3) **(Figure 1B; Supplemental Figure 2A-C)**. In contrast, the ligands for activating NK receptors, such as CD155 (ligand for DNAM1), MICA/B and ULBP1/2/3 (ligands for NKG2D) and B7-H6 (ligand for NKp30) were

upregulated on GSCs but not on healthy human astrocytes **(Figure 1B; Supplemental Figure 2A-C)**. In addition, using single cell RNA sequencing (scRNA seq) data generated by Darmanis et al. (19), we found that NK cell activating ligands are also abundantly expressed on non-GSC neoplastic cells **(Supplemental Figure 2D)**, supporting their susceptibility to NK cell-mediated killing. To assess the contributions of these activating and inhibitory receptors to the NK cell-dependent cytotoxicity against GSCs, we used receptor-specific blocking antibodies to disrupt specific receptor-ligand interactions. The blockade of NKG2D, DNAM1 and NKp30 but not HLA class I, significantly decreased NK cell-mediated GSC killing (n=4) **(Figure 1C)**. Cumulatively, these findings suggest that GSCs possess the ligands needed to stimulate NK cell activation leading to GSC elimination. Indeed, the effects we observed were entirely consistent with an extant model of tumor cell attack by NK cells, whereby inhibitory signals transmitted by KIR-HLA class I interactions are overcome when a threshold level of activating signals are reached, inducing recognition of 'stressed' cells (20, 21).

NK cells infiltrate GBM tumors but display an altered phenotype and function

Preclinical findings in glioma-bearing mice indicate that NK cells can cross the blood-brain barrier to infiltrate the brain (22). However, the limited clinical studies available suggest only minimal NK cell infiltration into GBM tissue (23). As such, we next investigated whether NK cells are capable of infiltrating into GBMs and assessed their abundance by analyzing *ex vivo* resected glioma tumor specimen collected in 21 of 46 patients with primary or recurrent GBM (**Table 1**), and 2 of 5 patients with low-grade gliomas **(Table 2)**. The patient characteristics are summarized in **Table 1** and **Table 2**. Each gram of GBM contained a median of 166,666 NK cells (range 9,520-600,000; n=21) whereas there were only 500-833 NK cells/g in low-grade gliomas (n=2). These findings indicate that NK cells can traffic into the GBM microenvironment in numbers that appear to be much larger in

high-grade gliomas. We also confirmed the presence of NK cells within the GBM immune microenvironment of patients with different tumor molecular subtypes using the GBM TCGA dataset **(Supplemental Figure 3)** as also reported by others (24).

To gain insights into the phenotype of the GBM tumor-infiltrating NK cells (TI-NKs), we used cytometry by time-of-flight (CyToF) and a panel of 37 antibodies against inhibitory and activating receptors, as well as differentiation, homing and activation markers **(Supplemental Table 1)**. We ran uniform manifold approximation and projection (UMAP) a dimensionality reduction method, on a dataset from paired GBM peripheral blood NK cells (GP-NK) and TI-NKs from patients with GBM and peripheral blood from healthy controls. Heatmap was used to compare protein expression between the groups. This analysis identified 4 main clusters **(Figure 1D-E)**. While GP-NK from patient with GBM and PB from healthy control (HC-NK) showed great phenotypic similarity, they were markedly different than TI-NKs, with the latter characterized by increased expression of $CD56^{bright}$, upregulation of inhibitory receptors such as KLRG-1, PD-1 and CD94 (which binds to both NKG2A and NKG2C) and significantly lower levels of activating receptors (CD16, NKG2D, NKp30, NKp46, DNAM-1, NKG2C, CD2, CD3ζ and 2B4), transcription factors (T-bet, eomes), signal transducing adaptor proteins (DAP10, DAP12, SAP) and cytotoxic molecules (granzyme B and perforin) as confirmed by mass cytometry **(Figure 1E; Supplemental Figure 4)** and by multi-parameter flow cytometry in TI-NKs and paired PB NK cells from 28 patients with GBM compared to PB samples from 15 HC **(Supplemental Figure 5A-C)**.

Next, we investigated the NK cell transcriptomic profile of TI-NKs from 10 additional glioma patients and PBMCs from healthy donors using a Drop-Seq-based scRNA-seq technology (10× Genomics STAR Methods) from a soon to be publicly available dataset of CD45+

glioma infiltrating immune cells [Zamler et al. Immune landscape of genetically-engineered murine models of glioma relative to human glioma by single-cell sequencing *Manuscript in Submission.* (2020)]. We analyzed over 1746 NK cells from each patient with GBM sample and over 530 cells from each healthy PBMC donor. The NK signature used to define the NK population included the markers KLRD1, NKG7 and NKTR. Uniform Manifold Approximation and Projection (UMAP)-based analysis revealed segregation in cell clusters of TI-NKs and HC-NK cells **(Figure 1F)**. There was significant downregulation of genes that encoded NK cell activation markers such as *NCR3* [NKp30], *GZMA* [granzyme A], *GZMK* [granzyme K], *SELL* [CD62L], *FCGR3A* [CD16] and *CD247* [CD3Z] in TI-NKs from patients with GBM compared with healthy donor PBMCs (HC-NK) **(Figure 1G; Supplemental Figure 5D)**. Genes that encoded for NK cell inhibitory receptors such as *KLRD1* [CD94], *KIR2DL1* and *KIR2DL4* were upregulated in the TI-NKs compared to the HC-NKs **(Figure 1G; Supplemental Figure 5D)**. Interestingly, genes associated with the TGF-β pathway, such as *JUND*, *SMAD7* and *SMURF2* were also significantly upregulated in TI-NKs compared with HC-NK **(Figure 1G; Supplemental Figure 5D)**.

We next tested the impact of our phenotypic findings on NK cell function by isolating NK cells from the GBM tumor (TI-NKs) or GP-NK cells from patients with GBM and from healthy donors (HC-NK) and testing their effector function against K562 targets. TI-NKs failed to kill K562 targets by ^{51}Cr release assay, had less degranulation (reduced expression of CD107a) and produced significantly lower amounts of IFN-γ and TNF-α than did GP- or HC-NK **(Figure 2A-B; Supplemental Figure 6)**. Taken together, these data indicate that NK cells can indeed migrate into GBMs but they undergo immune alteration within the tumor microenvironment that results in marked impairment of their cytotoxic function, indicating their susceptibility to immune evasion tactics of the malignant tumor.

TGF-β1 mediates NK cell dysfunction in GBM tumors

Despite the intrinsic sensitivity of GSCs to immune attack by NK cells, our findings indicate that this sensitivity is partially lost within the tumor microenvironment, where TI-NKs are modulated toward an inhibitory phenotype. Although there are many different mechanisms that could account for this shift in function (13), the TI-NKs phenotypic and single cell transcriptomic alterations were most consistent with the effects of *TGF-β1,* a pleiotropic cytokine that functions as an important inhibitor of the mTOR pathway (25). This notion was supported by the observation of enhanced basal levels of p-Smad2/3, the canonical TGF-β signaling pathway, in TI-NKs cells compared to GP-NK cells from patients with GBM or HC-NK cells **(Figure 2C; Supplemental Figure 7)**.

Given the rarity of the GSCs and their exquisite sensitivity to NK cell cytotoxicity, we reasoned that they may have evolved their own mechanisms of immune evasion in addition to the evasive tactics provided by the known immunoregulatory cells in the microenvironment (13). To pursue this hypothesis, we first tested whether GSCs can suppress the function of healthy allogeneic NK cells *in vitro* after co-culture for 48 hours. Co-incubation with normal astrocytes was used as control. After the co-culture period, the NK cells were harvested and purified by bead selection and their ability to kill GSC targets was assessed in a 4-hour ^{51}Cr release assay. While incubation with healthy human astrocytes (control) had no effect on NK cell function (n=3) **(Figure 2D; Supplemental Figure 8A)**, co-culture with patient-derived GSCs significantly impaired the ability of allogeneic NK cells to perform natural cytotoxicity and to produce IFN-γ and TNF-α in response to K562 targets (n=10; n=15 respectively) **(Figure 2E-F; Supplemental Figure 8B**). Next, we tested whether TGF-β plays a role in GSC-induced NK cells dysfunction by co-culturing NK cells from healthy control donors with patient-derived GSCs in the presence or absence of TGF-β neutralizing antibodies and assessing their cytotoxicity

against K562 targets. While the antibodies did not affect the normal function of healthy NK cells when cultured alone **(Supplemental Figure 9A)**, the blockade of TGF-β1 prevented GSCs from impairing NK cell cytotoxicity **(Supplemental Figure 9B-D)**. Thus, we conclude that TGF-β1 production by GSCs contributes significantly to NK cell dysfunction in the GBM microenvironment.

Disruption of TGF-β1 signaling prevents but does not reverse GSC-induced NK cell dysfunction

If GSCs induce NK cell dysfunction through release and extracellular activation of TGF-β1, it may be possible to avoid this evasive tactic by inhibiting the TGF-β signaling pathway. Thus, we first tested whether galunisertib (LY2157299), a TGF-β receptor I kinase inhibitor that has been used safely in patients with GBM (26), and LY2109761, a dual inhibitor of TGF-β receptors I and II, (27, 28) can prevent or reverse GSC-induced NK cell dysfunction. Although neither inhibitor affected NK cell function **(Supplemental Figure–10A)**, each prevented GSCs from activating the TGF-β1 Smad2/3 signaling pathway in NK cells **(Figure 3A)** and inducing dysfunction, thus preserving the natural cytotoxicity of NK cells against K562 or GSC targets **(Figure 3B; Supplemental Figure 10B-C)**. Interestingly, blockade of the TGF-β receptor kinase by galunisertib or *ex vivo* culture of TI-NKs with activating cytokines such as IL-15 failed to inactivate the TGF-β1 Smad2/3 signaling pathway and restore NK cell dysfunction **(Figure 3C**; **Supplemental Figure 10D-E)**. Similarly, these maneuvers did not reverse the dysfunction of HC-NK cells induced by GSCs **(Supplemental Figure 10F-G)** indicating that once NK cells are rendered dysfunctional in the suppressive microenvironment of GBM tumors, stimulation with IL-15 or inhibition of TGF-β1 activity is unlikely to restore their function.

GSCs induce NK cell dysfunction through cell-cell contact dependent TGF-β release

We next asked if latent TGF-β1 complex secretion by GSCs is an endogenous process, as observed with macrophages and myeloid-derived suppressor cells (MDSCs) (29, 30), or requires active cell-cell interaction with NK cells. To address this question, we performed transwell experiments in which healthy donor-derived NK cells and GSCs were either in direct contact with each other or separated by a 0.4 μm pore-sized permeable membrane that allowed the diffusion of soluble molecules, but not cells. Levels of total TGF-β1 were measured 48 hours after the cultures were initiated. Direct contact of GSCs with NK cells resulted in significantly higher levels of TGF-β1 compared with those attained when GSCs were separated from NK cells by a transwell (mean 836.9 pg/ml ± 333.1 S.D. vs 349 pg/ml ± 272.2 S.D.) or when GSCs were cultured alone (252 ± 190.4 pg/ml; $p<0.0001$) **(Figure 3D)**, indicating that release and activation of TGF-β by GSCs is a dynamic process requiring direct cell-cell contact between the NK cells and GSCs. Importantly, healthy human astrocytes cultured either alone or with NK cells did not produce substantial amounts of TGF-β1 **(Figure 3E)**. Consistent with these results, we found that GSC-mediated NK cell dysfunction also required direct cell-cell contact. Indeed, abrogation of direct cell-cell contact between NK cells and GSCs by a transwell membrane prevented the induction of NK cell dysfunction, and activation of the TGF-β1 Smad2/3 pathway, similar to results with TGF-β1 blocking antibodies **(Figure 3F-G; Supplemental Figure 11)**.

TGF-β1 is a tripartite complex and its inactive latent form is complexed with two other polypeptides: latent TGF-β binding protein (LTBP) and latency-associated peptide (LAP). Activation of the mature TGF-β1 requires its dissociation from the sequestering LAP. Because TGF-β1-LAP is expressed on the surface of GSCs at high levels **(Supplemental Figure 12A-B)**, we asked if the increase in total TGF-β levels in the supernatant after GSC-NK cell contact was driven by release of the cytokine from the sequestering LAP or

by increased transcription of the *TGFB1* gene, or both. To distinguish between these two alternatives, we investigated if contact with NK cells can induce a rapid release of TGF-β from LAP by measuring the kinetics of TGF-β1 production in the supernatant after GSC-NK cell co-culture. The results indicate a rapid increase in total TGF-β1 levels in the supernatant as early as 1 hour after co-culture in conditions where NK cells and GSCs were in direct contact compared with co-cultures in which NK cells and GSCs were cultured alone **(Figure 3H).** When the fold-changes in *TGFB1* mRNA were determined by quantitative PCR (qPCR) in GSCs alone or in direct contact with NK cells or separated from NK cells by a transwell membrane for 48 hours, the *TGFB1* copy numbers were significantly higher in GSCs in direct contact with NK cells ($p = 0.04$) **(Figure 3I)**. Thus, the marked increase in TGF-β1 seen after NK cell interaction with GSCs appears to involve a dual mechanism of upregulated *TGFB1* transcription and release of the mature cytokine from the LAP peptide by GSCs.

MMP2 and MMP9 play a critical role in the release of activated TGF-β1 from LAP

Both matrix metalloproteinases (MMPs) 2 and 9 mediate the release of TGF-β1 from LAP (31, 32). Because both enzymes are expressed by malignant gliomas (33), we investigated whether they might also be involved in the release of TGF-β1 from LAP and consequently in the induction of NK cell dysfunction by GSCs. First, we confirmed that GSCs are a major source of MMP2 and MMP9 **(Supplemental Figure 13A-B)**, and then determined their contribution to the release of TGF-β1 and GSC-induced NK cell dysfunction by culturing healthy NK cells with or without GSCs and in the presence or absence of an MMP2/9 inhibitor for 48 hours. MMPs were present at higher levels when GSCs were in direct contact with NK cells, suggesting that TGF-β1 drives their release, as confirmed by experiments using TGF-β blocking antibodies **(Supplemental Figure 13A-B)**. The addition of an MMP2/9 inhibitor did not affect NK cell function in cultures

lacking GSCs **(Supplemental Figure 13C)** but partially prevented GSC-induced NK dysfunction, as measured by the ability of the NK cells to perform natural cytotoxicity and to produce IFN-γ and TNF-α in response to K562 targets **(Supplemental Figure 13D-F).** This partial restoration would be consistent with the involvement of additional pathways in the activation of TGF-β. Incubation of NK cells with the MMP2/9 inhibitor also resulted in a moderate decrease in total TGF-β and significantly lower p-Smad2/3 levels **(Supplemental Figure 13G-H)**, implicating MMP2/9 in the release of TGF-β by GSCs.

αv integrins mediate cell contact dependent TGF-β1 release by GSCs

Since GSC-mediated NK cell dysfunction requires direct cell-cell contact, we next investigated which receptor-ligand interactions could be participating in this crosstalk. Blocking the interaction of major activating and inhibitory NK cell receptors, including CD155/CD112, CD44, KIRs and ILT-2, on healthy donor NK cells and their respective ligands on GSCs failed to prevent GSC-induced NK cell dysfunction **(Supplemental Figure 14)**. We then changed our focus to the integrins, a family of cell surface transmembrane receptors that play a critical role not only in cell adhesion, migration and angiogenesis, but also in the activation of latent TGF-β1(34). The αv (CD51) integrin heterodimeric complexes αvβ3, αvβ5 and αvβ8 are highly expressed in glioblastoma, in particular on GSCs (35). Based on evidence that targeting αv integrins in glioblastoma can significantly decrease TGF-β production,(35) we tested whether cilengitide, a small molecule inhibitor that possesses a cyclic RDG peptide with high affinity for αv integrins (αvβ3 and αvβ5) can prevent GSC-induced NK cell dysfunction by decreasing TGF-β1 production. Treatment with cilengitide significantly decreased levels of total TGF-β1 in the supernatant **(Figure 4A)** as well as p-Smad2/3 signaling in NK cells in direct contact with GSCs **(Figure 4B)** and protected NK cell from GSC-induced NK cell dysfunction (n=8; n=12) **(Figure 4C-E)**. These results were confirmed by genetic silencing of the pan-αv

integrin (*CD51*) in GSCs using CRISPR/Cas9 **(Figure 4F; Supplemental Figure 15).** Together, our data support a model in which αv integrins regulate the TGF-β1 axis involved in GSC-induced NK cell dysfunction **(see graphical abstract)**.

We next sought to identify the surface ligands on NK cells that could potentially interact with αv integrins to mediate GSC-NK cell crosstalk. In addition to binding extracellular matrix components, αv integrins bind tetraspanins, such as CD9, through their active RDG binding site (36). Indeed, CD9 and CD103 are upregulated on GBM TI-NKs **(Supplemental Figures 4 and 5)** and can be induced on healthy NK cells after co-culture with TGF-β1 **(Supplemental Figure 16A)**. Thus, we used CRISPR Cas9 gene editing to knockout (KO) *CD9* and *CD103* in healthy donor NK cells **(Supplemental Figure 16B)** and tested the cytotoxicity of wild type (WT, treated with Cas9 only), *CD9* KO, *CD103* KO or *CD9/CD103* double KO NK cells after co-culture with GSCs. As shown in **Supplemental Figure 16C-E,** silencing of either *CD9* or *CD103* resulted in partial improvement in the cytotoxic function of NK cells co-cultured with GSCs by comparison with WT control. In contrast, CD9/CD103 double KO NK cells co-cultured with GSCs retained their cytotoxicity against K562 targets **(Supplemental Figure 16C-E)**. This suggests that αv integrins on GSCs bind CD9 and CD103 on NK cells to regulate the TGF-β1 axis involved in GSC-induced NK cell dysfunction.

Inhibition of the αv integrin TGF-β1 axis enhances NK cell anti-tumor activity *in vivo*

The mechanistic insights gained from the above studies suggest that the αV integrin-TGF-β1 axis regulates an important evasion tactic used by GSCs to suppress NK cell cytotoxic activity and therefore may provide a useful target for immunotherapy of high-grade GBM. To test this prediction, we used two PDX mouse models of patient-derived GSC, in which,

ffLuc+ patient-derived GSCs (0.5 x 10^6 of GSC20 or GSC272) were stereotactically implanted on day 0 through a guide-screw into the right forebrain of NOD/SCID/IL2Rγc null mice (n=4-5 per group) and the αv integrin TGF-β1 axis was interrupted using either an αv integrin inhibitor, a TGF-β receptor kinase inhibitor or by genetic disruption of *TGFBR2* using CRISPR Cas9 gene editing **(Figure 5; Supplemental Figure 17)**. The GSC derived PDX mouse models were confirmed to be invasive **(Supplemental Figure 18)** as previously reported by Sadahiro et al (37). We first tested if the combination of NK cells with either galunisertib to block the TGF-β signaling or cilengitide to block the integrin pathway improves the antitumor response. Seven days after tumor implantation, the mice were treated intratumorally with 2.0×10^6 human NK cells every 7 days for 11 weeks **(Figure 5A)**. Galunisertib was administered five times a week by oral gavage and cilengitide three times a week by intraperitoneal injection. Animals implanted with tumor that were either untreated or received NK cells alone, galunisertib alone or cilengitide alone served as controls.

As shown in **Figure 5B and Supplemental Figure 17A**, tumor bioluminescence, used as a surrogate to assess tumor progression, rapidly increased in untreated mice and in mice that were treated with the monotherapies cilengitide or galunisertib. By contrast, weekly administration of NK cells either alone ($p<0.0001$) or combined with cilengitide or galunisertib (both $p<0.0001$) led to significant improvements in tumor control compared with untreated controls **(Figure 5B-C and Supplemental Figure 17A-B).** The best overall survival was observed when mice received NK cells combined with galunisertib ($p=0.009$) or with cilengitide ($p=0.05$) compared with untreated controls **(Figure 5D)**. Similar results were also noted with the more aggressive GSC272 mouse model **(Supplemental Figure 17)**. Immunohistochemical staining of brain specimen harvested from the animals confirmed infiltration by NK cells and direct cell-cell contact with GSCs **(Supplemental**

Figure 19). Moreover, no evidence of tissue damage or meningoencephalitis was noted in mice treated with human allogeneic NK cells plus cilengitide or galunisertib **(Supplemental Figure 20**). In animals that received adoptive NK cell infusion combined with cilengitide, TI-NKs harvested after mice were sacrificed showed a higher expression of NKG2D and reduced levels of CD9 and CD103; in contrast, NK cells harvested from animals treated with NK cells alone had a dysfunctional phenotype with lower expression of markers related to effector function (CD107a, perforin) **(Supplemental Figure 21)**. Since weekly administration of NK cells is very invasive, we explored a longer-term approach to protecting NK cells from GSC-induced NK cell dysfunction by testing the impact of *TGFBR2* KO **(Supplemental Figure 22).** As shown in **Figure 5F**, *in vitro* culture of wild type (WT) NK cells for 48 hours with recombinant TGF-β (10 ng/ml) resulted in downregulation of activating receptors and co-receptors (CD16, NKG2D, NKG2C, DNAM, NKp30, CD2 and 2B4), and upregulation of inhibitory receptors (TIM3, KIR). In contrast, *TGFBR2* KO NK cells treated with recombinant TGF-β did not show significant changes in their phenotype **(Figure 5E-F)**, transcriptomic profile **(Supplemental Figure 23A-C)** or cytotoxicity against K562 targets **(Figure 5G; Supplemental Figure 23D)**. Next, we analyzed the *in vivo* anti-tumor activity of *TGFBR2* KO NK cells by treating mice intracranially at day 7 post tumor implantation with either WT NK cells, WT NK cells plus galunisertib, or *TGFBR2* KO NK cells followed by subsequent NK cell injections every 4 weeks through a guide screw **(Figure 5H)**. In this model NK cells were administered less frequently (every 4 weeks) as a less invasive and more clinically translational approach. Tumor bioluminescence increased rapidly in untreated mice (GSC alone), while adoptive transfer of WT NK cells in combination with 5 x per week galunisertib or *TGFBR2* KO NK cells led to significant tumor control as measured by bioluminescence imaging **(Figure 5I-J)**. However, only treatment with *TGFBR2 KO* NK cells resulted in a significant improvement in the overall survival of the animals when compared to either untreated

controls (p=0.009) or animals treated with WT NK cells (p=0.01) **(Figure 5K)**. Treatment with 4-weekly injections of NK cells alone or NK cells in combination with 5 x day galunisertib failed to result in a significant increase in the survival of the animals when compared with untreated controls **(Figure 5K)**. In conclusion, our data support a combinatorial approach of NK cell adoptive therapy together with disruption of the αv integrin-TGF-β1 axis to target GBM.

DISCUSSION

Glioblastoma is among the most deadly and most difficult to treat of all human cancers. This difficulty can be in part attributed to the presence of GSCs that differ from their mature progeny in numerous ways, including resistance to standard chemotherapy and radiotherapy, and the ability to initiate tumors and mediate recurrence following treatment. Thus, unless the GSCs within the high-grade GBM tumors are eliminated, the possibility of cure is unlikely. Here, we show the critical importance of NK cells for GBM immunosurveillance, as demonstrated by the exquisite intrinsic sensitivity of GSCs to NK cell mediated killing and the notable influx of NK cells in the GBM microenvironment. This study is notable because its findings are based largely on profiling of primary tumor-infiltrating NK cells at the single cell level in tumor samples from patients with GBM, allowing a head-to-head comparison with key markers in peripheral blood and direct *ex vivo* functional assessment within an individual patient. Thus, such comparisons of NK cell transcriptomes in patients revealed a shift in gene-expression profiles indicative of a functional compromise with upregulation of inhibitory molecules and downregulation of activating molecules and systematic activation of genes related to the TGF-β pathway. This finding is consistent with a recent study in which NK cells in GBM tumors displayed an inhibitory gene expression profile with hallmarks of TGF-β-mediated inhibition. (38)

TGF-β is abundantly present in the GBM microenvironment and is released by the tumor as well as several other cell types, such as regulatory T cells, M2 macrophages and myeloid derived suppressor cells.(29, 30, 38-42) Although this cytokine is a well-characterized potent suppressor of NK cell functions(43), its mechanism of release and its contribution to GSC-induced NK cell dysfunction has remained unclear. Our working hypothesis of how GSCs evade NK cell recognition is summarized in **graphical abstract.** We propose that disruption of the blood-brain barrier caused by the tumor allows NK cells

to migrate into the GBM tumor tissue, where they interact with GSCs, inducing both the release and the production of TGF-β by GSCs in a cell-cell contact-dependent manner that requires interaction between αv integrins on GSCs and CD9 and CD103 on NK cells. TGF-β is then cleaved from its latent complex form to its biologically active form by proteases, such as MMP-2 and MMP-9, released mainly by GSCs. The release of these matrix metalloprotease is further driven by αv integrins and by TGF-β itself, as shown by data presented here and elsewhere (44-50). TGF-β, in turn irreversibly suppresses the cytotoxic function of NK cells by inducing changes in their phenotype, transcription factors, cytotoxic molecules and chemokines.

An important aspect of our model is the cross-talk between the αv integrins on GSCs and the TGF-β-induced receptors CD9 and CD103 on NK cells, acting as the main mediators of TGF-β production and subsequent NK cell dysfunction. Indeed, TGF-β has been reported to enhance CD103 inside-out signaling, further underscoring the complex interplay between TGF-β, CD103 and CD9 (51). We confirmed that silencing the pan-αv integrin (CD51) in GSCs by CRISPR/Cas9 gene editing or pharmacologic inhibition with cilengitide prevented GSC-induced NK cell dysfunction, diminished Smad2/3 phosphorylation and decreased TGF-β production in co-cultures of GSCs and NK cells. The αv integrins have been proposed to modulate latent TGF-β activation through two different mechanisms: (i) an MMP-dependent mechanism based on the production of MMP2 and MMP9 by glioma cells and GSCs, but not healthy brain tissue(33), leading to proteolytic cleavage TGF-β from LAP and (ii), an MMP-independent mechanism, that relies on cell traction forces (44, 47, 49, 50, 52). This duality may explain why the MMP-2/9 inhibitors used in this study could only partially protect NK cells from GSC-induced dysfunction.

Although a number of small molecules that globally inhibit TGF-β are in development for glioblastoma patients, most have been associated with prohibitive toxicity (53). In addition, the negative clinical data with cilengitide in GBM (54) may be at least partly explained by our observation that TGF-β inhibition prevents, but does not reverse, the state of established NK cell dysfunction induced by TGF-β in the tumor microenvironment. Taken together, these data support a combinatorial approach of NK cell immunotherapy with TGF-β or αv integrin inhibitors such as cilengitide to block TGF-β signaling by GSCs. Alternatively, gene editing strategies to delete the *TGFBR2* in NK cells could be used to protect against TGF-β binding and consequent immunosuppression. With either of these strategies, it should be possible to target local immunosuppressive mechanisms only, thus reducing the risk of excessive toxicity. It should be stressed that while both weekly unmodified NK cells and NK cells plus galunisertib or cilengitide could mediate effective antitumor responses **(Figure 5C, Supplemental Figure 17)**, when the interval of therapy was increased to every 4 weeks, the unmodified NK cells failed and only *TGFBR2* KO NK cells were capable of controlling the tumor **(Figure 5K)**. This observation supports our *in vitro* data that while it is expected to see some short-term anti-tumor activity of healthy allogeneic NK cells after adoptive transfer, when the interval of administration is increased (once every 4 weeks), unmodified NK cells lose their ability to control the tumor as they become susceptible to GSC-mediated immune evasion through the release of TGF-β. The genetically modified NK cells appear to be therapeutically superior relative to the combination of NK cells with a TGF-β receptor small molecule inhibitor, possibly because the inhibitor is subjected to pharmacokinetic and pharmacodynamic parameters that influence bioavailability in the CNS and thus efficacy in the GBM microenvironment.

Finally, on the strength of these findings, we propose to develop an immunotherapeutic strategy in which third-party NK cells derived from healthy donors are administered in

combination with a pan-αv integrin inhibitor or are genetically edited to silence *TGFBR2* to protect them from immunosuppression, thus, enabling them to recognize and eliminate tumor cells with stem-like properties such as GSCs.

MATERIALS AND METHODS

Patients

Forty-six patients with GBM (n=34 primary GBM; n=12 recurrent GBM) and five patients with low-grade glioma (n=2 low-grade oligodendroglioma; n=3 diffuse astrocytoma) were recruited from The University of Texas MD Anderson Cancer Center (MDACC) for phenotypic (n=28), functional studies (n=14) and single cell RNA sequencing analysis (n=10) **(Table 1** and **Table 2)**. Buffy coat from normal donors was obtained from gulf Coast Regional Blood Center, Houston, Texas, USA.

Characterization of GBM tumor infiltrating NK cells (TI-NKs), GBM peripheral blood NK cells (GP-NK) and healthy control NK cells (HC-NK)

Flow cytometry: Freshly isolated TI-NKs, GP-NK and HC-NK cells were incubated for 20 minutes at room temperature with Live/Dead-Aqua (Invitrogen) and surface markers. For detection of intracellular markers, cells were fixed/permeabilized using BD FACS lysing solution and permeabilizing solution 2 according to manufacturer's instructions (BD Biosciences) followed by intracellular staining for 30 minutes in room temperature. All data were acquired with BD-Fortessa (BD Biosciences) and analyzed with FlowJo software. The gating strategy for detection of NK cells is presented in **Supplemental Figure 24.** Details on the antibodies used in these studies are provided on the Supplemental Methods.

Mass Cytometry

The strategy for antibody conjugation is described elsewhere (55). **Supplemental Table 1** shows the list of antibodies used for the characterization of NK cells in the study. See Supplemental Methods for more details.

Single cell RNA sequencing

Details on the protocol are included in the Supplemental Methods. Our dataset was deposited and can be found below (Accession number-GSE147275): https://www.ncbi.nlm.nih.gov/geo/query/acc.cgi?acc=GSE147275.

To compare the GSC to non-GSC (well differentiated, mature GBM cells), we used previous data generated by Darmanis et al. (19). As described in that paper, we used *EGFR* and *SOX9* to first identify neoplastic GBM cells and then *SOX2, POU3F2*, *OLIG2*, and *SALL2* to identify GSCs while the remaining were defined as mature cells. We obtained *53* GSCs and 1038 non-GSC events for the analysis. We compared the expression of genes for the following NK cell receptor ligands: MICA/B, ULBP1-6, B7-H6, MLL-5, Vimentin, HLA-E, HLA-ABC, CD113, CD111, HLA-DR, PCNA, NID-1, HLA-G, CEACAM-1, LGALS9, CD112, CD155, BAG6/BAT3, CD48 and HLA-F and performed unpaired t test for statistical significance.

GSC culture

GSCs were obtained from primary human GBM samples as previously described (56, 57). The GSCs were cultured in stem cell-permissive medium (neurosphere medium): Dulbecco's Modified Eagle Medium containing 20 ng/ml of epidermal growth factor and basic fibroblast growth factor (all from Sigma-Aldrich), B27 (1:50; Invitrogen, Carlsbad, CA), 100 units/ ml of penicillin and 100 mg/ml streptomycin (Thermo Fisher Scientific, Waltham, MA) and passaged every 5–7 days (58). All generated GSC cell lines used in this paper were generated at MD Anderson Cancer Center and referred to as MDA-GSC.

Characterization of GSCs and human astrocytes

Human fetal astrocytes cell lines were purchased from Lonza (CC-2565) and Thermo Fisher Scientific (N7805100); the human glioblastoma U87 cell line (HTB-14) and the human astroglia cell line (CRL-8621) were purchased from the American Type Culture Collection (ATCC). The cells were separated into single cell suspension using accutase (Thermo Fisher Scientific) for GSCs and trypsin for the attached astrocytes. The cells were then stained for 20 minutes before washing and acquiring by flow cytometry (Details on the antibodies are provided in the Supplemental Methods).

NK cell cytotoxicity assays

NK cell functional and cytotoxicity assays were measured by cytokine production, NK cell degranulation, Incucyte real-time assay and chromium release assay. More details of these assays are provided in the Supplemental Methods. In addition to patient-derived GSCs generated from GBM tissue specimens at our institution, K562 (ATCC CCL-243, human erythroleukemia) cells were also used as targets for killing assays.

Transwell assays

NK cells (1x 10^5) were either added directly to GSCs at a ratio of 1:1 or placed in transwell chambers (Millicell, 0.4 μm; Millipore) for 48 hours at 37°C. After 48 hours, cultured cells were harvested to measure NK cell cytotoxicity by both ^{51}Cr release assay and cytokine secretion assay.

TGF-β ELISA and MMP2/9 luminex

NK cells and GSCs were either co-cultured or cultured alone for 48 hours in serum free SCGM growth medium. After 48 hours, supernatants were collected and the secretion of TGF-β and MMP2/3/9 was assessed in the supernatant by TGF-β1 ELISA kit (R&D

systems) or MMP2/3/9 luminex kit (eBiosciences) as per the manufacturer's protocol. For the TGF-β1 ELISA, activation was performed with 1N HCl for 10 minutes followed by neutralization with 1.2 N NaOH/0.5 M HEPES prior to sample utilization.

CRISPR gene editing of primary NK cells and GSCs

crRNAs to target *CD9*, *CD103* and *CD51* were designed using the Integrated DNA Technologies (IDT) predesigned data set. Guides with the highest on-target score and lowest off-target effect were selected. The crRNA sequences are reported in **Supplemental Table 2**. For more details see Supplemental Methods.

To knockout *TGFBR*2, two sgRNA guides (**Supplemental Table 2**) spanning close regions of exon 5 were designed and ordered from IDT; 1 µg cas9 (PNA Bio) and 500 ng of each sgRNA were incubated on ice for 20 minutes. After 20 minutes, NK cells 250,000 were added and re-suspended in T-buffer to a total volume of 14ul (Neon Electroporation Kit, Invitrogen) and electroporated before transfer to culture plate with APCs.

Xenogeneic mouse model of GBM

To assess the anti-tumor effect of NK cells against GSCs *in vivo*, we used a NOD/SCID IL-2Rγnull (NSG) human xenograft model (Jackson Laboratories, Bar Harbor, ME). We have used a patient derived GSC mouse model due to their superior invasiveness and migratory ability relative to conventional glioma cell lines when implanted intracranially(37). Intracranial implantation of GSCs into male mice was performed as previously described(59). A total of 140 mice were used, 0.5×10^6 patient-derived GSC20 or GSC272 were implanted intracranially into the right frontal lobe of 5 week old NSG mice using a guide-screw system implanted within the skull. To increase uniformity of xenograft uptake and growth, cells were injected into 10 animals simultaneously using a multiport

Microinfusion Syringe Pump (Harvard Apparatus, Holliston, MA). Animals were anesthetized with xylazine/ketamine during the procedure. For *in vivo* bioluminescent imaging, GSCs were engineered to express luciferase by lentivirus transduction. Kinetics of tumor growth was monitored using weekly bioluminescence imaging (BLI; Xenogen-IVIS 200 Imaging system; Caliper, Waltham, MA). Signal quantitation in photons/second (p/s) was performed by determining the photon flux rate within standardized regions of interest (ROI) using Living Image software (Caliper). $2x10^6$ in 3 µl expanded donor peripheral blood NK cells (60) were injected intracranially via the guide-screw at day 7 post tumor implantation, and then every 7 days for 11 weeks for GSC20 and 6 weeks for GSC272. Mice were treated with either cilengitide or galunisertib (both from MCE Med Chem Express, Monmouth Junction, NJ) in the presence or absence of intracranial NK cell injection. Cytokines were not administered to the mice *in vivo* but rather they received multiple doses of expanded NK cells. Cilengitide was administered intraperitoneally 3 times a week starting at day 1 (250 µg/100 µl PBS) while galunisertib was administered orally (75 mg/kg) by gavage 5 days a week starting at day 1 (see **Figure 5A**). For GSC272, mice were treated with either cilenglitide, galunisertib with or without NK cells and with *TGFBR2* KO NK cells. In another experiment, mice were injected intracranially via the guide screw 7 days post tumor inoculation with either wild type (WT) NK cells, WT NK cells plus galunisertib or *TGFBR2* KO NK cells followed by subsequent NK cells injections every 4 weeks as describe above. Mice that presented neurological symptoms (i.e. hydrocephalus, seizures, inactivity, and/or ataxia) or moribund were euthanized. Brain tissue was then extracted and processed for NK cells extraction.

Statistical analyses

Statistical significance was assessed with SPSS version 26 (IBM) and Prism 9.0 software (GraphPad Software, Inc.). Means were compared using unpaired t-test, paired t-test, two-

way ANOVA or repeated measures ANOVA. The Dunnett correction was used when comparing to a category of reference or control, otherwise we used the Tukey correction. Additionally, the Bonferroni correction was used to adjust for repeated measures. For survival comparison a Log-rank test was used. Graphs represent mean and standard deviation (SD). A $P \leq 0.05$ was considered to be statistical significance. When analyzing variables with more than 2 categories, P values were adjusted for multiple comparisons.

Study Approval

All Tumor tissues that were used for the generation of glioma stem cells were resected from patients who signed written informed consents and samples were collected in accordance with the Institutional Review Board of The University of Texas MD Anderson Cancer Center in Houston IRB Protocol LAB04-0001 and LAB03-0687. All tissue samples were de-indentified. All studies were performed in accordance with the Declaration of Helsinki. All animal experiments were performed in accordance with recommendations in the Guide for the Care and Use of Laboratory Animals of the National Institute of Health, and approved by the Institutional Animal Care and Use Committee (IACUC) protocol number 00001263-RN01 at MD Anderson Cancer Center in Houston.

ACKNOWLEDMENTS

We thank our summer students Nadia Agha (University of Houston), Cindy Saliba (University of Iowa) and Lihi Shalev (Hebrew University of Jerusalem) for their assistance with some of the experiments performed in the paper.

FUNDING

This research was made possible by the generous support of Ann and Clarence Cazalot. This work was also supported in part by the Dr. Marnie Rose Foundation and the generous

philanthropic contributions to The University of Texas MD Anderson Cancer Center Glioblastoma Moonshot Program, by grants (CA016672; CA120813) to the MD Anderson Cancer Center from the NIH and by the Specialized Program of Research Excellence (SPORE) in Brain Cancer grant (P50CA127001). The MD Anderson Flow Cytometry and Cellular Imaging Core Facility (FCCICF), NCI Cancer Center Support Grant (P30CA16672) assisted with the CyTOF studies in this project.

AUTHOR CONTRIBUTIONS

HS, MS and RB performed experiments, interpreted and analyzed data. KG, YH, JG, AA, NU, SL, JJL, SA, EG, JY, NWF, LL, MK, MB, AKNC, ELE, DZ, ALG, CMJ, LNK and YL assisted with experiments and commented on the manuscript. KC, FW, QM, JD, YS and VM performed statistical analysis and commented on the manuscript. KG and CK provided clinical data. MD, JW, MM, LL, MM, EJS, PPB, EL, DY, REC, MB, SM, GO, NI, ME, MK, JH, GD and FL provided advice on experiments and commented on the manuscript. KR and AH designed and directed the study. HS, RB, KR, DM, MS and LMF wrote the manuscript.

COMPETING INTERESTS

HS, MS, RB, EJS and KR have filed for a patent: MDA 20-021; UTSC.P1190US.P1; "Natural killer cell immunotherapy for the treatment of glioblastoma." KR, EJS, REC, EL, RB, MD, PPB, DM and The University of Texas MD Anderson Cancer Center (MDACC) have an institutional financial conflict of interest with Takeda Pharmaceutical for the licensing of the technology related to CAR-NK cells. MD Anderson has implemented an Institutional Conflict of Interest Management and Monitoring Plan to manage and monitor the conflict of interest with respect to MDACC's conduct of any other ongoing or future

research related to this relationship. KR, EJS, RB, EL, DM and The University of Texas MD Anderson Cancer Center has an institutional financial conflict of interest with Affimed GmbH. Because MD Anderson is committed to the protection of human subjects and the effective management of its financial conflicts of interest in relation to its research activities, MD Anderson is implementing an Institutional Conflict of Interest Management and Monitoring Plan to manage and monitor the conflict of interest with respect to MD Anderson's conduct of any other ongoing or future research related to this relationship. KR participates on Scientific Advisory Board for GemoAb, AvengeBio, Kiadis, GSK and Bayer. The other authors declare no potential conflicts of interest.

DATA AVAILABILITY

The data that support the findings of this manuscript are available from the corresponding author upon reasonable request.

TABLES

Table 1: Characteristics of patients with GBM.

Patien numb	Sex	Age DO	Histolog	NK cell count/gra tissue	IDH1 status	MGMT status	TP53 status	EGFR status	PTEN Status	ATRX Loss	Previous Treatment (Time from last treatment to surgery)	Assay utilization
1	M	57	pGBM	N/A	N/A	N/A	N/A	N/A	N/A	N/A	none	phenotype, functional (C+L)
2	M	46	pGBM	600,000	neg	N/A	pos	N/A	N/A	N/A	none	phenotype, functional (C+L)
3	M	54	rGBM	280,000	N/A	pos	N/A	N/A	N/A	N/A	RT+TMZ (7 weeks)	phenotype, functional (C+L)
4	M	45	pGBM	9,520	neg	N/A	pos	pos	pos	N/A	none	phenotype, functional (C)
5	M	66	pGBM	370,000	neg	pos	pos	N/A	N/A	N/A	none	phenotype, functional (C+L)
6	M	38	rGBM	N/A	pos	intermediat e	pos	N/A	N/A	N/A	RT+TMZ (unknown)	phenotype, functional (C), p-smad
7	M	32	rGBM*	N/A	pos	N/A	pos	N/A	N/A	N/A	Accutane, RT+TMZ (3 weeks)	Phenotype, p-smad
8	F	80	pGBM	N/A	N/A	N/A	N/A	N/A	N/A	N/A	none	phenotype, functional (C), p-smad
9	M	62	pGBM	200,000	neg	N/A	pos	N/A	N/A	N/A	none	phenotype, functional (L), p-smad
10	F	51	pGBM	200,000	neg	pos	pos	pos	N/A	N/A	none	phenotype, p-smad
11	M	56	pGBM	N/A	neg	neg	pos	N/A	N/A	N/A	none	phenotype
12	F	30	rGBM	300,000	pos	pos	pos	N/A	N/A	N/A	XRT+TMZ (6 weeks)	Phenotype, p-smad
13	F	55	pGBM	N/A	neg	N/A	pos	pos	pos	N/A	none	phenotype
14	F	64	pGBM	166,666	neg	N/A	pos	N/A	pos	N/A	none	phenotype
15	M	31	pGBM	133,333	neg	pos	N/A	N/A	N/A	N/A	none	functional (L)
16	F	43	pGBM	100,000	pos	pos	pos	pos	neg	N/A	none	phenotype
17	M	60	pGBM	N/A	neg	neg	N/A	pos	pos	N/A	none	phenotype
18	M	67	pGBM	N/A	neg	neg	N/A	pos	neg	N/A	none	phenotype, functional (C), reversal
19	F	42	pGBM	N/A	neg	pos	pos	pos	N/A	N/A	none	phenotype
20	M	54	rGBM	N/A	neg	neg	pos	N/A	N/A	N/A	RT+TMZ (6 weeks)	phenotype
21	M	54	rGBM	N/A	neg	N/A	pos	pos	pos	N/A	RT+TMZ (8 weeks)	functional (C), reversal
22	M	73	pGBM	266,666	neg	pos	pos	pos	mixed	N/A	none	phenotype, reversal
23	M	56	rGBM	N/A	N/A	N/A	N/A	N/A	N/A	N/A	XRT+ RT+ Lomustin and avastin (6 weeks)	p-smad
24	F	50	pGBM	N/A	neg	N/A	N/A	N/A	N/A	N/A	none	phenotype
25	M	62	pGBM	166,666	N/A	N/A	N/A	N/A	N/A	N/A	none	reversal
26	F	60	pGBM	N/A	neg	pos	N/A	pos	neg	N/A	none	phenotype
27	F	42	pGBM	N/A	N/A	neg	pos	pos	pos	neg	none	reversal
28	M	56	pGBM	116,666	neg	neg	pos	pos	neg	neg	none	functional (C)
29	M	71	pGBM	N/A	neg	neg	pos	pos	N/A	N/A	none	functional (L)
30	M	68	rGBM	N/A	neg	neg	pos	pos	neg	neg	RT+ TMZ (3 weeks)	functional (L)
31	M	71	pGBM	N/A	neg	pos	pos	pos	neg	pos	none	phenotype
32	M	50	pGBM	350,000	neg	neg	neg	N/A	neg	neg	none	phenotype
33	F	61	pGBM	250,000	neg	N/A	pos	N/A	neg	neg	none	p-smad
34	M	42	pGBM	200,000	neg	neg	pos	neg	neg	neg	none	p-smad
35	M	50	rGBM	40,000	neg	neg	neg	neg	N/A	neg	RT+ TMZ (5 ½ weeks)	phenotype, p-smad
36	F	40	pGBM	166,666	pos	pos	pos	pos	N/A	neg	none	reversal
37	F	65	pGBM	35,000	neg	pos	pos	pos	pos	neg	none	phenotype
38	M	64	pGBM	142,857	neg	neg	pos	pos	N/A	neg	none	phenotype

39	F	31	rGBM	60,000	neg	neg	pos	neg	pos	pos	RT+TMZ (4 weeks)	phenotype
40	M	65	pGBM	N/A	neg	N/A	neg	N/A	N/A	neg	none	scRNA seq
41	M	53	pGBM	N/A	neg	N/A	pos	N/A	N/A	neg	none	scRNA seq
42	M	52	pGBM	N/A	neg	N/A	pos	N/A	N/A	neg	none	scRNA seq
43	M	66	pGBM	N/A	neg	neg	pos	N/A	N/A	N/A	none	scRNA seq
44	F	70	pGBM	N/A	neg	N/A	pos	N/A	N/A	neg	none	scRNA seq
45	M	71	rGBM	N/A	neg	pos	N/A	pos	N/A	neg	TMZ+RT + enrolled in PVSRIPO (1 ½ years)	scRNA seq
46	M	71	rGBM	N/A	neg	neg	N/A	N/A	N/A	neg	TMZ + RT (6 weeks)	scRNA seq

Abbreviations:
Pos=positive; neg= negative; DOS= day of surgery; pGBM= primary GBM; rGBM= recurrent GBM; TMZ=temozolomide; XRT=photon radiotherapy; RT= radiotherapy; R= Reversal of NK cell dysfunction: *ex vivo* expansion and culture with cytokines +/- galunisertib to assess the reversal of NK cell dysfunction; Functional: cytokine assay (C) or NK cell lysis (L); scRNA seq= single cell RNA sequencing; PVSRIPO= recombinant nonpathogenic polio–rhinovirus chimera. N/A= data not available.

* Arose from low grade glioma

Table 2: Characteristics of patients with low-grade glioma.

Patient	Sex	Age at DOS	Histology	NK cell count/gram tissue	IDH1 status	MGMT status	TP53 status	Previous treatment	Assay utilization
1	F	34	Low grade oligodendroglioma	500	pos	pos	pos	none	none
2	M	27	Diffuse astrocytoma	833	neg	N/A	neg	none	none
3	M	60	Low grade oligodendroglioma	N/A	pos	N/A	N/A	none	scRNA seq
4	F	45	Diffuse astrocytoma	N/A	pos	pos	pos	none	scRNA seq
5	M	39	Diffuse astrocytoma	N/A	pos	neg	pos	none	scRNA seq

Abbreviations:
pos= positive; neg= negative; DOS= day of surgery; scRNA seq= single cell RNA sequencing. N/A=data not available.

FIGURES

Figure 1

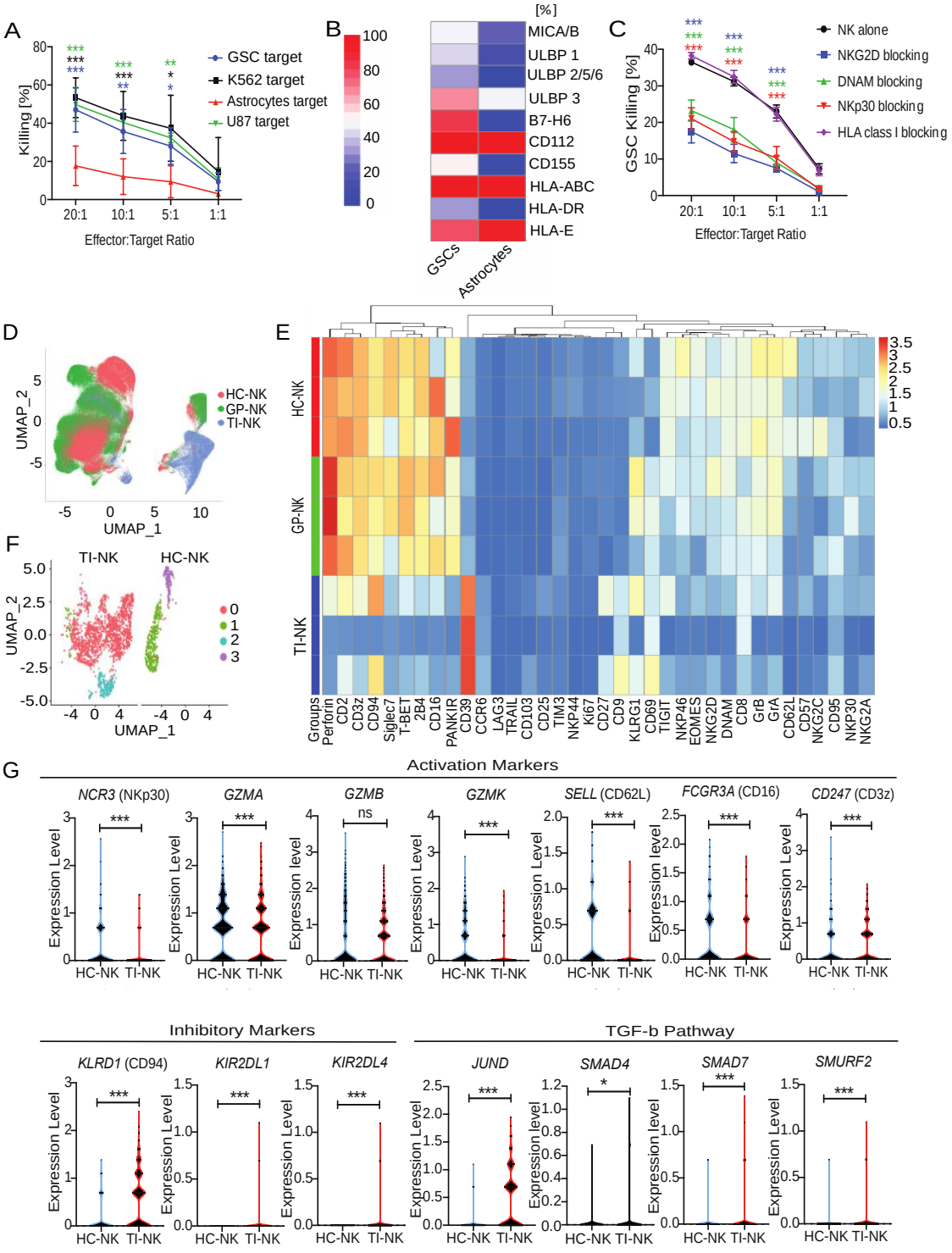

Figure 1. GSCs express NK cell receptor ligands and are susceptible to NK cell cytotoxicity. A, ^{51}Cr-release assay showing cytotoxicity of donor-derived NK cells activated overnight with IL-15 (5 ng/ml) against GSCs (blue), K562 (black), U87 cell line (green) or healthy human astrocytes (red). (U87: n=3; K562, GSCs, astrocytes: n=6). Error bars denote SD; Green*: cytotoxicity against U87 vs. astrocytes, black*: cytotoxicity against K562 vs. astrocytes. Blue*: cytotoxicity against GSCs vs. astrocytes; B, Heat map representing the relative expression of NK cell ligands on GSCs or human astrocytes ranging from blue (low) to red (high). Columns represent the median expression of each receptor (GSC: n=6; Astrocytes: n=3); C, Activated HC-NK were co-cultured with GSCs in the presence or absence of blocking antibodies: anti-NKG2D (blue), anti-DNAM (green), anti-NKp30 (red) or anti-HLA class I (purple). ^{51}Cr-release assay against GSCs was assessed (n=4). Blue*: cytotoxicity against GSC with or without anti-NKG2D, Red*: cytotoxicity against GSC with or without anti-NKp30, Green*: cytotoxicity against GSC with or without anti-DNAM. D, E, viSNE plots (D) and a comparative mass cytometry heatmap (E) showing the expression of NK cell markers in HC-NK (red), GP-NK (green) and TI-NK (blue). Column clustering is identified by FlowSOM. Each row reflects annotation of the expression level for an individual patient. Color scale ranges from blue lower expression to red higher expression (n=3). F, UMAP plot showing clusters for TI-NKs versus HC-NK by scRNAseq. G, Violin plots showing the mRNA expression levels for individual NK cell related genes in healthy control (HC-NK; blue) and TI-NK (red) using scRNAseq. Markers associated with NK cell activation and cytotoxicity, inhibition and the TGF-β pathway are presented. Statistical analysis by 2-way ANOVA with Dunnett's correction for multiple comparisons (A, C) or unpaired t-test (G). * $p \leq 0.05$, ** $p \leq 0.01$, *** $p \leq 0.001$.

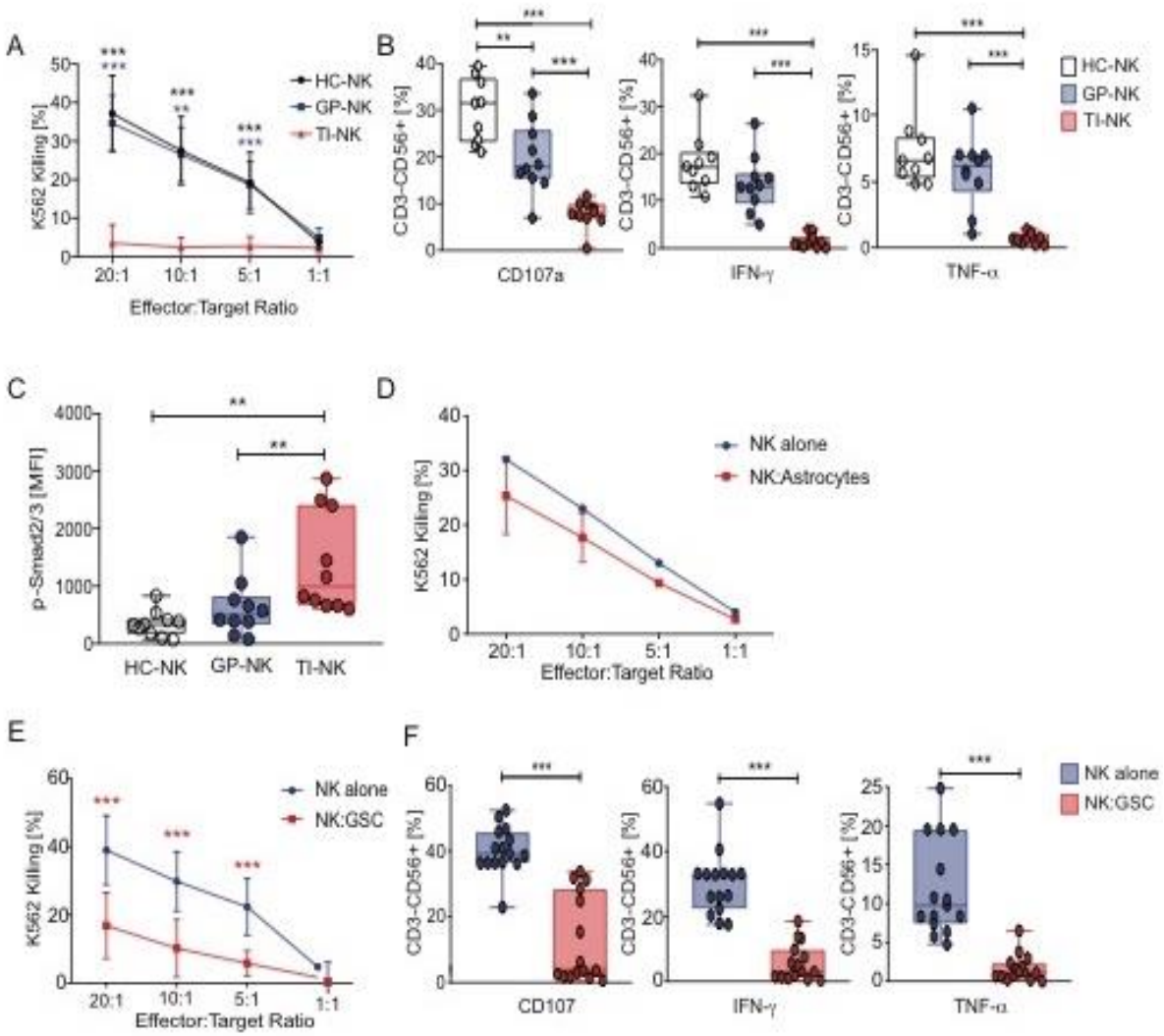

Figure 2. GSCs induce NK cell dysfunction. A, Primary human GBM tumor infiltrating NK cells (TI-NK) (red), paired peripheral blood NK cells (GP-NK) (blue) from the same patient with GBM or peripheral blood NK cells from healthy control donor (HC-NK) (black) were co-cultured for 4 hours with K562 at different ratios and the cytotoxicity was determined by ^{51}Cr release assay (n=8). Black*: HC-NK cell cytotoxicity against K562 targets vs. TI-NK. Blue*: GP-NK cell cytotoxicity against K562 vs. paired TI-NK. B, Box plots summarizing CD107a, IFN-γ, and TNF-α production by TI-NK, GP-NK or HC-NK cells after incubation with K562 for 5 hours at a 5:1 ratio (n=10). C, Comparison of the

mean fluorescence intensity (MFI) of p-Smad2/3 expression in NK cells from healthy controls (HC-NK, white), GP-NK (blue) and TI-NKs (red) (n=10). D, Susceptibility of K562 to NK cells that were co-cultured at a 1:1 ratio with healthy astrocytes (red) or alone (blue) for 48 hours. NK cells were then purified and their ability to kill K562 targets was assessed by ^{51}Cr release assay (n=3). E, Specific lysis (^{51}Cr release assay) of K562 cells by NK cells cultured alone or with GSCs at a 1:1 ratio for 48h (n=10); Red*: Statistical significance in NK cell cytotoxicity against K562 for NK cells co-cultured with GSCs vs. NK cells alone. F, Box plots summarizing CD107a, IFN-γ, and TNF-α production by NK cells cultured either alone or with GSCs in a 1:1 ratio for 48 hours in response to K562. (n=10). Statistical analysis by 2-way ANOVA with Dunnett's correction for multiple comparisons (A, C), 2-way ANOVA with Tukey's correction for multiple comparisons (B, D, E) or paired t-test (F). ** $p \leq 0.01$, *** $p \leq 0.001$.

Figure 3

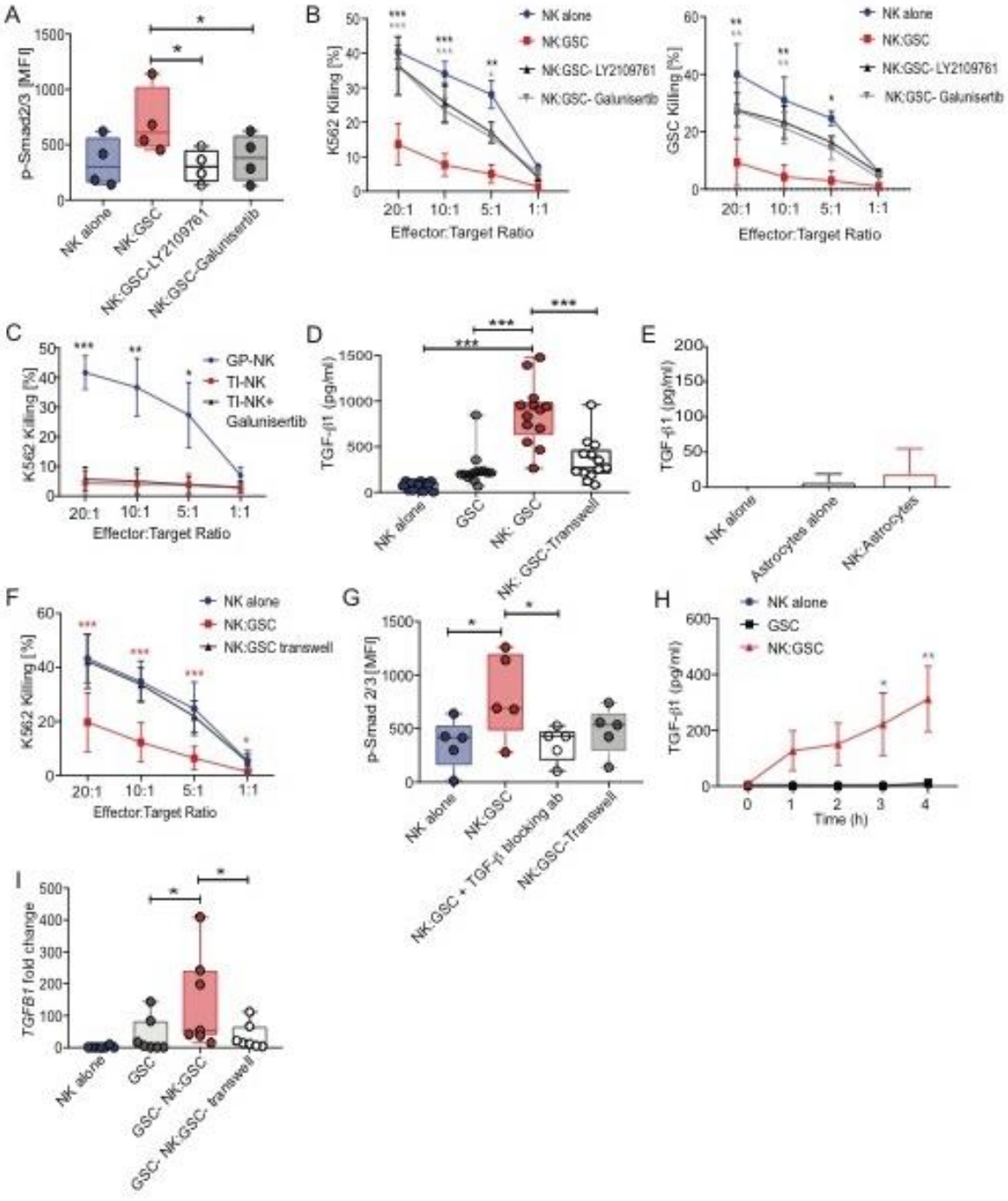
A
p-Smad2/3 [MFI]
NK alone
NK:GSC
NK:GSC-LY2109761
NK:GSC-Galunisertib
B
K562 Killing [%]
NK alone
NK:GSC
NK:GSC- LY2109761
NK:GSC- Galunisertib
20:1
10:1
5:1
1:1
Effector:Target Ratio
GSC Killing [%]
C
K562 Killing [%]
GP-NK
TI-NK
TI-NK+ Galunisertib
Effector:Target Ratio
D
TGF-β1 (pg/ml)
NK alone
GSC
NK: GSC
NK: GSC-Transwell
E
TGF-β1 (pg/ml)
NK alone
Astrocytes alone
NK:Astrocytes
F
K562 Killing [%]
NK alone
NK:GSC
NK:GSC transwell
Effector:Target Ratio
G
p-Smad 2/3 [MFI]
NK alone
NK:GSC
NK:GSC + TGF-β blocking ab
NK:GSC-Transwell
H
TGF-β1 (pg/ml)
NK alone
GSC
NK:GSC
Time (h)
I
TGFB1 fold change
NK alone
GSC
GSC- NK:GSC
GSC- NK:GSC- transwell

Figure 3. GSC-induced NK cell dysfunction requires cell-cell contact. A, p-Smad2/3 (MFI) expression in NK cells cultured alone or with GSCs in the presence or absence of LY2109761 or galunisertib; (n=4). B, HC-NK cells were cultured with or without GSCs for 48 hours in the presence or absence of LY2109761 or galunisertib. A 4-hour ^{51}Cr-release assay tested their cytotoxicity against K562 (left) or GSC (right) targets. Asterisks represent the statistical difference in NK cell cytotoxicity in the presence or absence of galunisertib (grey) or LY2109761 (black) (n=3). C, TI-NKs were cultured overnight with or without galunisertib and their cytotoxicity tested against K562 targets in a 4-hour ^{51}Cr-release assay. Black*: TI-NK+Galunisertib vs. GP-NK (n=3). D, E, Total TGF-β1 (pg/ml; ELISA) levels in supernatants from NK cells and GSCs cultured alone or together for 48 hours in direct contact or separated with a transwell membrane (D; n=13) or NK cells and astrocytes cultured alone or together for 48 hours (E; n=3). F, NK cells co-cultured with GSCs for 48 hours in direct contact or separated with a transwell and their cytotoxicity tested against K562 in a 4-hour ^{51}Cr-release assay (n=7). G, p-Smad2/3 (MFI) expression in HC-NK cells cultured overnight with or without GSCs in the presence or absence of TGF-β blocking antibodies, or separated with a transwell membrane (n=5). H, Total TGF-β1 (ELISA) in the supernatant of NK cells and GSCs cultured alone (NK: blue; GSC: black) or together (red) (n=4). Blue*: GSC vs. NK:GSC. I, Fold-change in *TGFB1* mRNA levels in NK cells and GSCs cultured for 48 hours either alone, or together in direct contact or separated with a transwell membrane (n=7). Statistical analysis by 2-way ANOVA with Dunnett's (A-C, E-H), Tukey's (D) or Bonferroni's correction for multiple comparisons (I). *p≤ 0.05, **p ≤ 0.01, ***p ≤ 0.001.

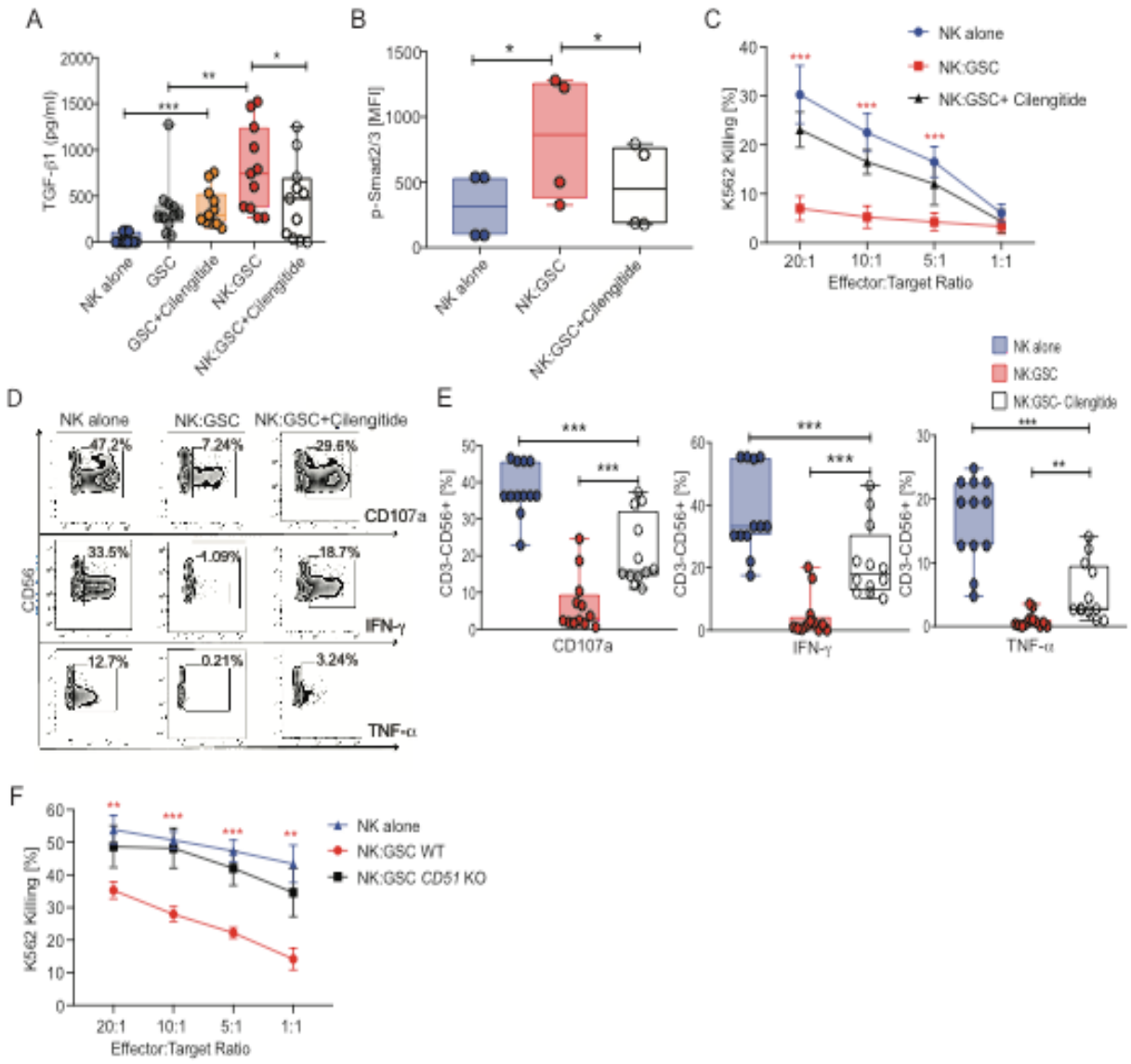

Figure 4. αv integrins mediate TGF-β1 release by GSCs and GSC-induced NK cell dysfunction. A, Box plots showing total TGF-β (pg/ml) in the supernatant of NK cells and GSCs cultured either alone or together in the presence or absence of the αv integrin small molecule inhibitor cilengitide (10 μM) for 48 hours was determined by ELISA (n=11). B, Box plots showing MFI of p-Smad2/3 expression on HC-NK cells cultured either alone or with GSCs in the presence or absence of cilengitide (10 μM). C, ^{51}Cr release assay of

K562 killing by NK cells cultured either alone or after co-culture with GSCs for 48 hrs in the presence or absence of cilengitide (10 μM) (n=8). Red*: specific lysis of K562 targets by NK cells that were cocultured with GSCs in the presence or absence cilengitide, D, E, Representative zebra plots (D) and summary box plots (E) of CD107, IFN-γ, and TNF-α production by NK cells in response to K562 cultured either alone or after 48 hrs of co-culture with GSCs at a 1:1 ratio with or without cilengitide (n=12). Inset numbers in panel D are the percentages of CD107a-, IFN-γ- or TNF-α-positive NK cells within the indicated regions. F, ^{51}Cr release assay of K562 targets by NK cells cultured either alone or with WT GSCs or with *CD51* KO GSCs for 48 hrs at a 1:1 ratio (n=3). Red*: the specific lysis of K562 targets by NK cells after coculture with WT GSCs vs. *CD51* KO. Statistical analysis by 2-way ANOVA with Bonferroni's correction for multiple comparisons (A, B, E, F) or 2-way ANOVA with Dunnett's correction for multiple comparisons (C). * $p \leq 0.05$, ** $p \leq 0.01$, *** $p \leq 0.001$.

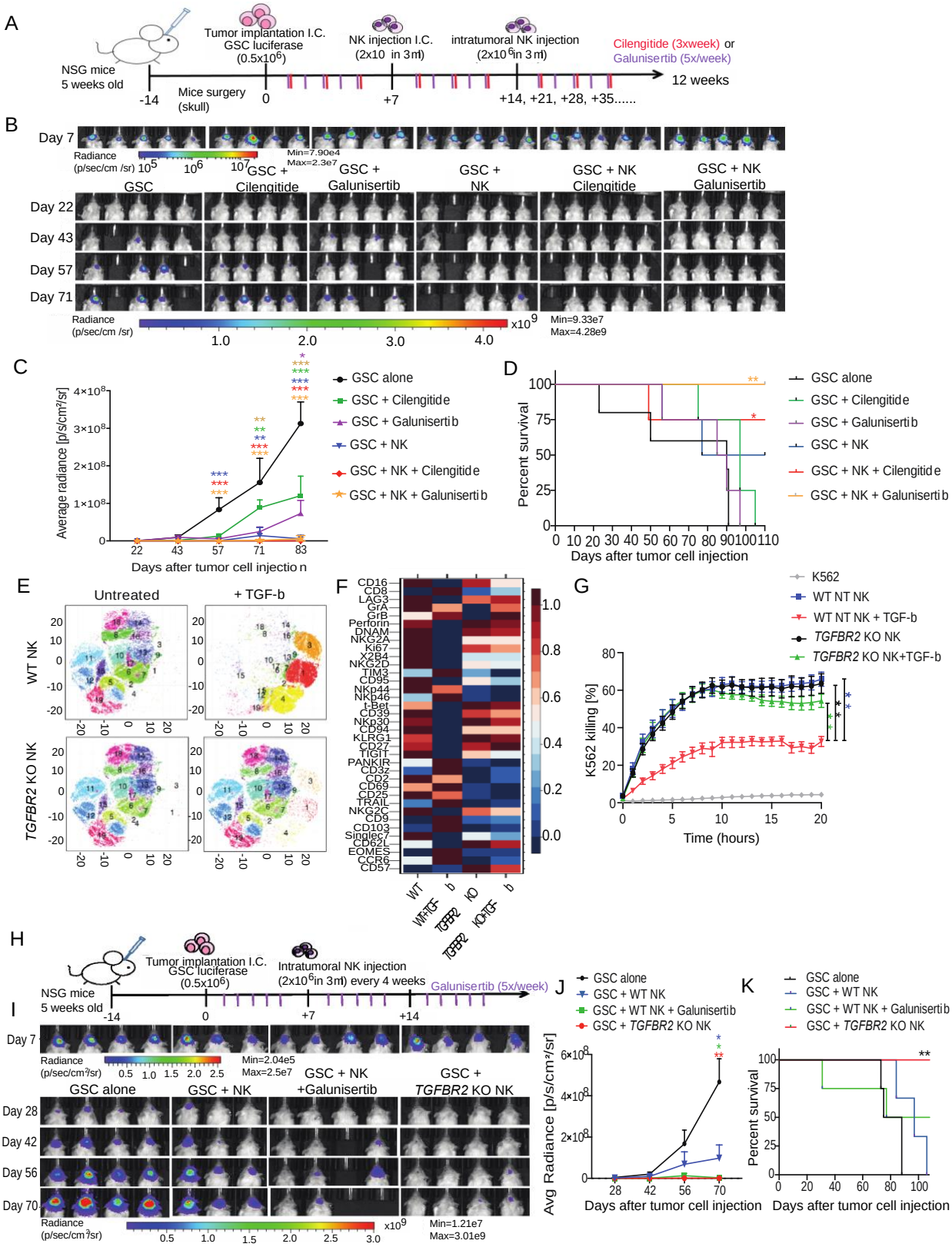
A
NSG mice
5 weeks old
Tumor implantation I.C.
GSC luciferase
(0.5x10^6)
NK injection I.C.
(2x10^6 in 3㎖)
intratumoral NK injection
(2x10^6 in 3㎖)
Cilengitide (3xweek) or
Galunisertib (5x/week)
12 weeks
-14
Mice surgery
(skull)
0
+7
+14, +21, +28, +35.....
B
Day 7
Radiance
(p/sec/cm /sr)
Min=7.90e4
Max=2.3e7
GSC
GSC + Cilengitide
GSC + Galunisertib
GSC + NK
GSC + NK Cilengitide
GSC + NK Galunisertib
Day 22
Day 43
Day 57
Day 71
Min=9.33e7
Max=4.28e9
C
Average radiance [p/s/cm²/sr]
Days after tumor cell injection
GSC alone
GSC + Cilengitide
GSC + Galunisertib
GSC + NK
GSC + NK + Cilengitide
GSC + NK + Galunisertib
D
Percent survival
Days after tumor cell injection
E
Untreated
+ TGF-b
WT NK
TGFBR2 KO NK
F
CD16
CD8
LAG3
GrA
GrB
Perforin
DNAM
NKG2A
Ki67
X2B4
NKG2D
TIM3
CD95
NKp44
NKp46
t-Bet
CD39
NKp30
CD94
KLRG1
CD27
TIGIT
PANKIR
CD32
CD2
CD69
CD25
TRAIL
NKG2C
CD9
CD103
Singlec7
CD62L
EOMES
CCR6
CD57
WT
WT+TGF-b
TGFBR2 KO
TGFBR2 KO+TGF-b
G
K562
WT NT NK
WT NT NK + TGF-b
TGFBR2 KO NK
TGFBR2 KO NK+TGF-b
K562 killing [%]
Time (hours)
H
NSG mice
5 weeks old
Tumor implantation I.C.
GSC luciferase
(0.5x10^6)
Intratumoral NK injection
(2x10^6 in 3㎖) every 4 weeks
Galunisertib (5x/week)
-14
0
+7
+14
I
Day 7
Radiance
(p/sec/cm²/sr)
Min=2.04e5
Max=2.5e7
GSC alone
GSC + NK
GSC + NK +Galunisertib
GSC + TGFBR2 KO NK
Day 28
Day 42
Day 56
Day 70
Min=1.21e7
Max=3.01e9
J
GSC alone
GSC + WT NK
GSC + WT NK + Galunisertib
GSC + TGFBR2 KO NK
Avg Radiance [p/s/cm²/sr]
Days after tumor cell injection
K
GSC alone
GSC + WT NK
GSC + WT NK + Galunisertib
GSC + TGFBR2 KO NK
Percent survival
Days after tumor cell injection

Figure 5. *In vivo* antitumor activity and NK cell function following TGF-β and αv integrin signaling inhibition in GBM mouse model. A, Schematic diagram showing the timeline of the *in vivo* experiment. B, Bioluminescence imaging (BLI) at different time points was used as a surrogate marker for tumor progression (n=4-5). C, Average radiance (BLI) data. Orange*: NK + galunisertib vs. tumor control. Red*: NK + cilengitide vs. tumor control. Blue*: NK alone vs. tumor control. Green*: NK + galunisertib vs. cilengitide control. Brown*: NK + cilengitide vs. cilengitide control. Purple*: NK + galunisertib vs. galunisertib control, D, Survival for mice in each group (n=5). Animals treated with NK + galunisertib or NK + cilengitide had a significantly better survival compared to tumor controls (p=0.009 and p=0.05, respectively). E, F, viSNE plots (E) and comparative heatmap (F) of mass cytometry data showing the expression of NK cell markers in WT *or TGFBR2* KO NK cells with or without recombinant TGF-β. Heatmap column clustering generated by FlowSOM analysis; color scale shows the expression of each marker, red (high) and blue (low). G, Killing of K562 over time by WT-NK (blue), *TGFBR*2 KO (black), WT-NK + recombinant TGF-β (red) or *TGFBR*2 NK + recombinant TGF-β (gray) as measured by real time killing assay. H, Schematic diagram showing the timeline of subsequent *in vivo* mouse experiment. I, BLI was obtained from the four groups of mice (n=4). J, Average radiance (BLI) data: Red*: *TGFBR*2 KO NK vs. tumor controls. Green*: WT NK + Galunisertib vs. tumor controls. Blue*: WT NK vs. tumor controls K, Kaplan-Meier plot showing mice survival. Statistical analysis by 2-way ANOVA with Dunnett's correction for multiple comparisons (C, G, J) or log-rank test (D, K). *p≤ 0.05, **p ≤ 0.01, ***p ≤ 0.001.

REFERENCES

1. Stupp R, Mason WP, van den Bent MJ, Weller M, Fisher B, Taphoorn MJ, et al. Radiotherapy plus concomitant and adjuvant temozolomide for glioblastoma. *N Engl J Med.* 2005;352(10):987-96.
2. Bao S, Wu Q, McLendon RE, Hao Y, Shi Q, Hjelmeland AB, et al. Glioma stem cells promote radioresistance by preferential activation of the DNA damage response. *Nature.* 2006;444(7120):756-60.
3. Lan X, Jorg DJ, Cavalli FMG, Richards LM, Nguyen LV, Vanner RJ, et al. Fate mapping of human glioblastoma reveals an invariant stem cell hierarchy. *Nature.* 2017;549(7671):227-32.
4. Guo M, Wu T, and Wan L. Cytotoxic activity of allogeneic natural killer cells on U251 glioma cells in vitro. *Mol Med Rep.* 2016;14(1):583-9.
5. Jung TY, Choi YD, Kim YH, Lee JJ, Kim HS, Kim JS, et al. Immunological characterization of glioblastoma cells for immunotherapy. *Anticancer Res.* 2013;33(6):2525-33.
6. Kang SG, Ryu CH, Jeun SS, Park CK, Shin HJ, Kim JH, et al. Lymphokine activated killer cells from umbilical cord blood show higher antitumor effect against anaplastic astrocytoma cell line (U87) and medulloblastoma cell line (TE671) than lymphokine activated killer cells from peripheral blood. *Childs Nerv Syst.* 2004;20(3):154-62.
7. Kondo S, Yin D, Takeuchi J, Morimura T, Miyatake SI, Nakatsu S, et al. Tumour necrosis factor-alpha induces an increase in susceptibility of human glioblastoma U87-MG cells to natural killer cell-mediated lysis. *Br J Cancer.* 1994;69(4):627-32.
8. Tanaka Y, Nakazawa T, Nakamura M, Nishimura F, Matsuda R, Omoto K, et al. Ex vivo-expanded highly purified natural killer cells in combination with temozolomide induce antitumor effects in human glioblastoma cells in vitro. *PLoS One.* 2019;14(3):e0212455.
9. Weiss T, Weller M, Guckenberger M, Sentman CL, and Roth P. NKG2D-Based CAR T Cells and Radiotherapy Exert Synergistic Efficacy in Glioblastoma. *Cancer Res.* 2018;78(4):1031-43.
10. Castriconi R, Daga A, Dondero A, Zona G, Poliani PL, Melotti A, et al. NK cells recognize and kill human glioblastoma cells with stem cell-like properties. *J Immunol.* 2009;182(6):3530-9.
11. Daher M, and Rezvani K. Next generation natural killer cells for cancer immunotherapy: the promise of genetic engineering. *Curr Opin Immunol.* 2018;51:146-53.
12. Rezvani K, and Rouce RH. The Application of Natural Killer Cell Immunotherapy for the Treatment of Cancer. *Front Immunol.* 2015;6:578.
13. Nduom EK, Weller M, and Heimberger AB. Immunosuppressive mechanisms in glioblastoma. *Neuro Oncol.* 2015;17 Suppl 7:vii9-vii14.
14. Gieryng A, Pszczolkowska D, Walentynowicz KA, Rajan WD, and Kaminska B. Immune microenvironment of gliomas. *Lab Invest.* 2017;97(5):498-518.

15. Beier CP, Kumar P, Meyer K, Leukel P, Bruttel V, Aschenbrenner I, et al. The cancer stem cell subtype determines immune infiltration of glioblastoma. *Stem Cells Dev.* 2012;21(15):2753-61.
16. Lottaz C, Beier D, Meyer K, Kumar P, Hermann A, Schwarz J, et al. Transcriptional profiles of CD133+ and CD133- glioblastoma-derived cancer stem cell lines suggest different cells of origin. *Cancer Res.* 2010;70(5):2030-40.
17. Shibao S, Minami N, Koike N, Fukui N, Yoshida K, Saya H, et al. Metabolic heterogeneity and plasticity of glioma stem cells in a mouse glioblastoma model. *Neuro Oncol.* 2018;20(3):343-54.
18. Nishimura M, Mitsunaga S, Akaza T, Mitomi Y, Tadokoro K, and Juji T. Protection against natural killer cells by interferon-gamma treatment of K562 cells cannot be explained by augmented major histocompatibility complex class I expression. *Immunology.* 1994;83(1):75-80.
19. Darmanis S, Sloan SA, Croote D, Mignardi M, Chernikova S, Samghababi P, et al. Single-Cell RNA-Seq Analysis of Infiltrating Neoplastic Cells at the Migrating Front of Human Glioblastoma. *Cell Rep.* 2017;21(5):1399-410.
20. Cerwenka A, Baron JL, and Lanier LL. Ectopic expression of retinoic acid early inducible-1 gene (RAE-1) permits natural killer cell-mediated rejection of a MHC class I-bearing tumor in vivo. *Proceedings of the National Academy of Sciences of the United States of America.* 2001;98(20):11521-6.
21. Zhang H, Cui Y, Voong N, Sabatino M, Stroncek DF, Morisot S, et al. Activating signals dominate inhibitory signals in CD137L/IL-15 activated natural killer cells. *Journal of immunotherapy.* 2011;34(2):187-95.
22. Tran Thang NN, Derouazi M, Philippin G, Arcidiaco S, Di Berardino-Besson W, Masson F, et al. Immune infiltration of spontaneous mouse astrocytomas is dominated by immunosuppressive cells from early stages of tumor development. *Cancer Res.* 2010;70(12):4829-39.
23. Kmiecik J, Poli A, Brons NH, Waha A, Eide GE, Enger PO, et al. Elevated CD3+ and CD8+ tumor-infiltrating immune cells correlate with prolonged survival in glioblastoma patients despite integrated immunosuppressive mechanisms in the tumor microenvironment and at the systemic level. *J Neuroimmunol.* 2013;264(1-2):71-83.
24. Zhong QY, Fan EX, Feng GY, Chen QY, Gou XX, Yue GJ, et al. A gene expression-based study on immune cell subtypes and glioma prognosis. *BMC Cancer.* 2019;19(1):1116.
25. Viel S, Marcais A, Guimaraes FS, Loftus R, Rabilloud J, Grau M, et al. TGF-beta inhibits the activation and functions of NK cells by repressing the mTOR pathway. *Sci Signal.* 2016;9(415):ra19.
26. Capper D, von Deimling A, Brandes AA, Carpentier AF, Kesari S, Sepulveda-Sanchez JM, et al. Biomarker and Histopathology Evaluation of Patients with Recurrent Glioblastoma Treated with Galunisertib, Lomustine, or the Combination of Galunisertib and Lomustine. *Int J Mol Sci.* 2017;18(5).
27. Brandes AA, Carpentier AF, Kesari S, Sepulveda-Sanchez JM, Wheeler HR, Chinot O, et al. A Phase II randomized study of galunisertib monotherapy or

galunisertib plus lomustine compared with lomustine monotherapy in patients with recurrent glioblastoma. *Neuro Oncol.* 2016;18(8):1146-56.
28. Zhang M, Kleber S, Rohrich M, Timke C, Han N, Tuettenberg J, et al. Blockade of TGF-beta signaling by the TGFbetaR-I kinase inhibitor LY2109761 enhances radiation response and prolongs survival in glioblastoma. *Cancer Res.* 2011;71(23):7155-67.
29. Gonzalez-Junca A, Driscoll KE, Pellicciotta I, Du S, Lo CH, Roy R, et al. Autocrine TGFbeta Is a Survival Factor for Monocytes and Drives Immunosuppressive Lineage Commitment. *Cancer Immunol Res.* 2019;7(2):306-20.
30. Liu Z, Kuang W, Zhou Q, and Zhang Y. TGF-beta1 secreted by M2 phenotype macrophages enhances the stemness and migration of glioma cells via the SMAD2/3 signalling pathway. *Int J Mol Med.* 2018;42(6):3395-403.
31. Kessenbrock K, Plaks V, and Werb Z. Matrix metalloproteinases: regulators of the tumor microenvironment. *Cell.* 2010;141(1):52-67.
32. Gialeli C, Theocharis AD, and Karamanos NK. Roles of matrix metalloproteinases in cancer progression and their pharmacological targeting. *FEBS J.* 2011;278(1):16-27.
33. Wang M, Wang T, Liu S, Yoshida D, and Teramoto A. The expression of matrix metalloproteinase-2 and -9 in human gliomas of different pathological grades. *Brain Tumor Pathol.* 2003;20(2):65-72.
34. Mamuya FA, and Duncan MK. aV integrins and TGF-beta-induced EMT: a circle of regulation. *J Cell Mol Med.* 2012;16(3):445-55.
35. Roth P, Silginer M, Goodman SL, Hasenbach K, Thies S, Maurer G, et al. Integrin control of the transforming growth factor-beta pathway in glioblastoma. *Brain.* 2013;136(Pt 2):564-76.
36. Yu J, Lee CY, Changou CA, Cedano-Prieto DM, Takada YK, and Takada Y. The CD9, CD81, and CD151 EC2 domains bind to the classical RGD-binding site of integrin alphavbeta3. *Biochem J.* 2017;474(4):589-96.
37. Sadahiro H, Yoshikawa K, Ideguchi M, Kajiwara K, Ishii A, Ikeda E, et al. Pathological features of highly invasive glioma stem cells in a mouse xenograft model. *Brain Tumor Pathol.* 2014;31(2):77-84.
38. Close HJ, Stead LF, Nsengimana J, Reilly KA, Droop A, Wurdak H, et al. Expression profiling of single cells and patient cohorts identifies multiple immunosuppressive pathways and an altered NK cell phenotype in glioblastoma. *Clin Exp Immunol.* 2020;200(1):33-44.
39. Tada T, Yabu K, and Kobayashi S. Detection of active form of transforming growth factor-beta in cerebrospinal fluid of patients with glioma. *Jpn J Cancer Res.* 1993;84(5):544-8.
40. Frei K, Gramatzki D, Tritschler I, Schroeder JJ, Espinoza L, Rushing EJ, et al. Transforming growth factor-beta pathway activity in glioblastoma. *Oncotarget.* 2015;6(8):5963-77.
41. Roy LO, Poirier MB, and Fortin D. Differential Expression and Clinical Significance of Transforming Growth Factor-Beta Isoforms in GBM Tumors. *Int J Mol Sci.* 2018;19(4).

42. Wan YY, and Flavell RA. 'Yin-Yang' functions of transforming growth factor-beta and T regulatory cells in immune regulation. *Immunol Rev.* 2007;220:199-213.
43. Dahmani A, and Delisle JS. TGF-beta in T Cell Biology: Implications for Cancer Immunotherapy. *Cancers (Basel).* 2018;10(6).
44. Wipff PJ, and Hinz B. Integrins and the activation of latent transforming growth factor beta1 - an intimate relationship. *Eur J Cell Biol.* 2008;87(8-9):601-15.
45. Gu X, Niu J, Dorahy DJ, Scott R, and Agrez MV. Integrin alpha(v)beta6-associated ERK2 mediates MMP-9 secretion in colon cancer cells. *Br J Cancer.* 2002;87(3):348-51.
46. Thomas GJ, Poomsawat S, Lewis MP, Hart IR, Speight PM, and Marshall JF. alpha v beta 6 Integrin upregulates matrix metalloproteinase 9 and promotes migration of normal oral keratinocytes. *J Invest Dermatol.* 2001;116(6):898-904.
47. Dutta A, Li J, Fedele C, Sayeed A, Singh A, Violette SM, et al. alphavbeta6 integrin is required for TGFbeta1-mediated matrix metalloproteinase2 expression. *Biochem J.* 2015;466(3):525-36.
48. Deryugina EI, Ratnikov B, Monosov E, Postnova TI, DiScipio R, Smith JW, et al. MT1-MMP initiates activation of pro-MMP-2 and integrin alphavbeta3 promotes maturation of MMP-2 in breast carcinoma cells. *Exp Cell Res.* 2001;263(2):209-23.
49. Kim ES, Kim MS, and Moon A. TGF-beta-induced upregulation of MMP-2 and MMP-9 depends on p38 MAPK, but not ERK signaling in MCF10A human breast epithelial cells. *Int J Oncol.* 2004;25(5):1375-82.
50. Hsieh HL, Wang HH, Wu WB, Chu PJ, and Yang CM. Transforming growth factor-beta1 induces matrix metalloproteinase-9 and cell migration in astrocytes: roles of ROS-dependent ERK- and JNK-NF-kappaB pathways. *J Neuroinflammation.* 2010;7:88.
51. Boutet M, Gauthier L, Leclerc M, Gros G, de Montpreville V, Theret N, et al. TGFbeta Signaling Intersects with CD103 Integrin Signaling to Promote T-Lymphocyte Accumulation and Antitumor Activity in the Lung Tumor Microenvironment. *Cancer research.* 2016;76(7):1757-69.
52. Wang J, Su Y, Iacob RE, Engen JR, and Springer TA. General structural features that regulate integrin affinity revealed by atypical alphaVbeta8. *Nature communications.* 2019;10(1):5481.
53. Herbertz S, Sawyer JS, Stauber AJ, Gueorguieva I, Driscoll KE, Estrem ST, et al. Clinical development of galunisertib (LY2157299 monohydrate), a small molecule inhibitor of transforming growth factor-beta signaling pathway. *Drug Des Devel Ther.* 2015;9:4479-99.
54. Stupp R, Hegi ME, Gorlia T, Erridge SC, Perry J, Hong YK, et al. Cilengitide combined with standard treatment for patients with newly diagnosed glioblastoma with methylated MGMT promoter (CENTRIC EORTC 26071-22072 study): a multicentre, randomised, open-label, phase 3 trial. *Lancet Oncol.* 2014;15(10):1100-8.

55. Li L, Chen H, Marin D, Xi Y, Miao Q, Lv J, et al. A novel immature natural killer cell subpopulation predicts relapse after cord blood transplantation. *Blood Adv.* 2019;3(23):4117-30.
56. Jiang H, Gomez-Manzano C, Aoki H, Alonso MM, Kondo S, McCormick F, et al. Examination of the therapeutic potential of Delta-24-RGD in brain tumor stem cells: role of autophagic cell death. *J Natl Cancer Inst.* 2007;99(18):1410-4.
57. Pollard SM, Yoshikawa K, Clarke ID, Danovi D, Stricker S, Russell R, et al. Glioma stem cell lines expanded in adherent culture have tumor-specific phenotypes and are suitable for chemical and genetic screens. *Cell stem cell.* 2009;4(6):568-80.
58. Gabrusiewicz K, Li X, Wei J, Hashimoto Y, Marisetty AL, Ott M, et al. Glioblastoma stem cell-derived exosomes induce M2 macrophages and PD-L1 expression on human monocytes. *Oncoimmunology.* 2018;7(4):e1412909.
59. Lal S, Lacroix M, Tofilon P, Fuller GN, Sawaya R, and Lang FF. An implantable guide-screw system for brain tumor studies in small animals. *J Neurosurg.* 2000;92(2):326-33.
60. Shah N, Martin-Antonio B, Yang H, Ku S, Lee DA, Cooper LJ, et al. Antigen presenting cell-mediated expansion of human umbilical cord blood yields log-scale expansion of natural killer cells with anti-myeloma activity. *PLoS One.* 2013;8(10):e76781.